HHS Public Access

Author manuscript

Immunity. Author manuscript; available in PMC 2024 October 10.

Published in final edited form as:

Immunity. 2023 October 10; 56(10): 2373–2387.e8. doi:10.1016/j.immuni.2023.08.018.

Antigen receptor signaling and cell death resistance controls intestinal humoral response zonation

Fiona Raso[1], **Shuozhi Liu**[2], **Mikala JoAnn Willett**[3], **Gregory Barton**[4], **Christian Thomas Mayer**[3], **Oliver Bannard**[5], **Mridu Acharya**[2,6], **Jagan R. Muppidi**[7], **Ann Marshak-Rothstein**[8], **Andrea Reboldi**[1,9,*]

[1]Department of Pathology, University of Massachusetts Chan Medical School, Worcester, MA

[2]Seattle Children's Research Institute, Seattle, WA

[3]Experimental Immunology Branch, Center for Cancer Research, NCI, NIH, Bethesda

[4]Department of Molecular and Cell Biology, University of California, Berkeley CA

[5]MRC Human Immunology Unit, Nuffield Department of Medicine, MRC Weatherall Institute of Molecular Medicine, University of Oxford

[6]Department of Pediatrics, University of Washington, Seattle, WA

[7]Lymphoid Malignancies Branch, Center for Cancer Research, NCI, NIH, Bethesda

[8]Department of Medicine, University of Massachusetts Chan Medical School, Worcester, MA

[9]Lead contact

Summary

Immunoglobulin A (IgA) maintains commensal communities in the intestine while preventing dysbiosis. IgA generated against intestinal microbes assures the simultaneous binding to multiple, diverse commensal-derived antigens. However, the exact mechanisms by which B cells mount broadly reactive IgA to the gut microbiome remains elusive. Here we have shown that IgA B cell receptor (BCR) is required for B cell fitness during the germinal center reaction in Peyer's patches and for generation of gut-homing plasma cells. We demonstrate that IgA BCR drove heightened intracellular signaling in mouse and human B cells and as a consequence, IgA^+ B cells received stronger positive selection cues. Mechanistically, IgA BCR signaling offset Fas-mediated death, possibly rescuing low affinity B cells to promote a broad humoral response to commensals.

*Correspondence: Andrea.Reboldi@umassmed.edu (A.R.).

AUTHOR CONTRIBUTIONS

F.R. and A.R. conceived the study, developed the concept, designed the experiments, and wrote the paper. F.R. performed experiments, analyzed the data, and interpreted the results. S.L., M.J.W. and O.B. performed experiments. C.T.M, J.R.M, O.B., and M.A. analyzed and interpreted the data. G.B. provided *Iga*$^{-/-}$ mice. A.M-R. provided FasL vesicles. All authors contributed to the review and editing of the manuscript. A.R. reviewed all data and supervised the research.

DECLARATIONS OF INTERESTS

The authors declare no competing interests.

Our findings reveal an additional mechanism linking BCR signaling, B cell fate, and antibody production location which have implications for how intestinal antigen recognition shapes humoral immunity.

Graphical Abstract

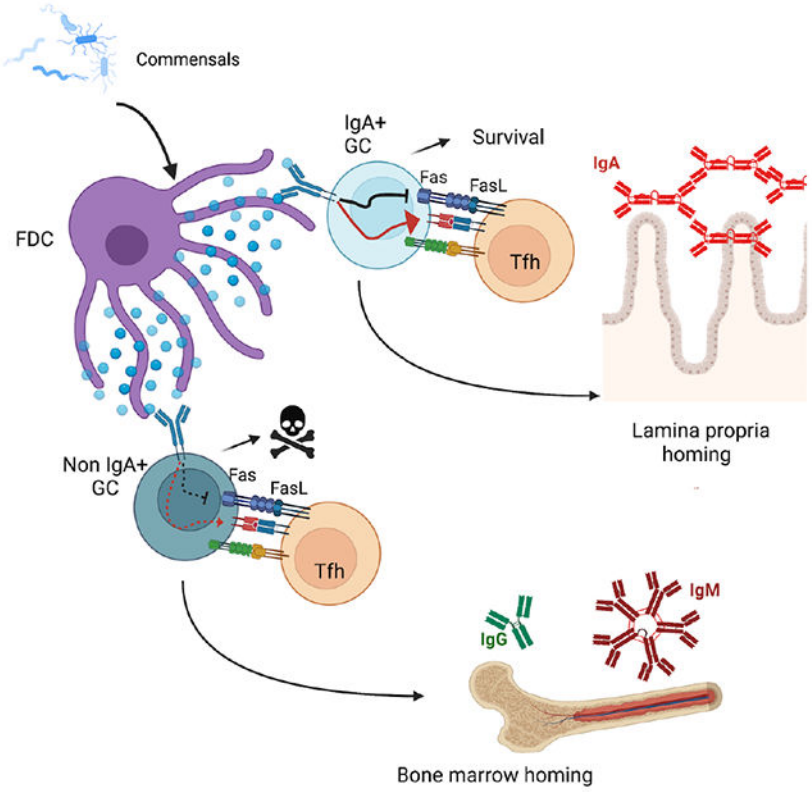

In brief

IgA response is critical for intestinal immunity, however the role of IgA during germinal center (GC) is unknown. Here, Raso et al. reveal that the IgA B cell receptor (BCR) is required for Peyer's patch (PP) GC B cell survival and selection into memory B cells and gut-homing plasma cells.

INTRODUCTION

Secretion of Immunoglobulin A (IgA) at the intestinal interface is critical to control the ecology of commensal communities: data from both murine and human studies indicate that deficiency in IgA responses alters the composition of the microbiome[1–3], leading to increased susceptibility to enteric pathogens and reduced tissue responses to oral vaccines.[4,5]

In recent years, the specificity of IgA has been the focus of intense investigation: it is accepted that a single IgA can bind multiple unrelated bacterial taxa[6–9] a property described as cross-species reactivity[10], but species-specific IgA also exist[11], and both processes contribute to widen IgA response to commensals. While IgA can coat commensals

in the absence of T cells[12–14], there is evidence that IgA selection is regulated by T cells.[15] Furthermore, IgA-secreting plasma cells in the intestine are highly mutated[16–20] and require affinity maturation to properly control commensals.[21] Somatic mutations and affinity maturation occur in the germinal center (GC) reaction and depend on T cell help, suggesting that GC may play an important role in establishing a functional intestinal IgA response. Peyer's patches (PPs)[22] are characterized by ongoing GC[23], and seminal work has identified them as the main site for the generation of IgA against intestinal antigens.[24,25] In PPs, tissue-resident cells produce environmental cues that enforce IgA class switch recombination before B cell entry into the GC[26–28], and control differentiation of antigen-specific plasma cells.[29] The GC reaction is primarily required for the selection of B cell clones binding antigen with high affinity, that eventually differentiate into antibody secreting plasma cells[30–32], a feature which is difficult to reconcile with the known broad reactivity of IgA. However, in contrast to peripheral lymph nodes (LNs) or spleen, GC regulation in PPs has been shown to be less dependent on positive and negative T follicular helper (Tfh) cell signals.[33,34] Moreover, recent data have highlighted that the complexity of gut microbiome shapes both affinity and clonality during the GC reaction: under homeostatic conditions, selection of highly dominant B cell clones is rare in PPs, a starkly different situation compared to peripheral LNs upon immunization.[30,35,36] Thus, a PP-specific mechanism must exist that modulates the GC reaction and underpins the generation of poly- or cross-species reactive intestinal IgA.

Following acquisition of activation-induced cytidine deaminase (AID)-mediated BCR point mutations, GC B cells test their mutated BCR for binding of antigen displayed by follicular dendritic cells and receive T cell help by cognate Tfh cells. The relative contribution of T cell help and BCR signaling in controlling GC selection has been debated[37–41]: the current view is that Tfh cells are central in discriminating between B cells carrying BCR with different affinities and they drive differentiation of high affinity B cells into plasma cells.[32] Nevertheless, several groups have reported that surface BCR isotypes can intrinsically modulate B cell differentiation, including selection during the GC reaction.[42–45]

The impact of IgA BCR in the GC reaction of PPs, and its effect on the humoral immune response at the intestinal barrier, remain largely unknown. In the present study, we examined the role of IgA in regulating chronic GC reactions in response to commensal and pathogenic bacteria. We found that IgA facilitated GC B cell fitness and was required for the generation of gut-homing plasma cells. IgA^+ B cells were positively selected in the light zone and were resistant to apoptosis. The IgA BCR mediated stronger intracellular signaling and offset FasL-dependent apoptosis. In conclusion, acquisition of an IgA BCR in PPs is not only required for the generation of low inflammatory antibodies that can be translocated into the lumen, but it also lowers the threshold of selection and might contribute to a broad response to commensals.

RESULTS

IgA$^+$ B cells dominate the germinal center reaction and are preferentially selected into the memory compartment.

We initially sought to evaluate whether surface IgA BCR was required for effective participation in the GC reaction. To this end, we used mice with a targeted deletion of the IgA switch region and sequence, which completely abolishes both IgA-expressing B cells and secreted IgA.[46] Immunohistochemical analysis of PPs did not reveal altered GC structure in the absence of IgA (Figure 1A), with normal size of the follicle and GC (Figure S1A). We then analyzed PP and mesenteric lymph node (mLN) B cell populations by flow cytometry for the distribution of follicular B cells (B220$^+$ IgD$^+$ GL7$^-$), GC B cells (B220$^+$ IgD- GL7$^+$), memory B cells (MemB, B220$^+$ IgD$^-$ GL7$^-$ CD38$^+$ CD138$^-$), and plasma cells (PCs, IgD$^-$ GL7$^-$ CD138$^+$) (Figure 1B, S1B). No difference in B cell subsets was observed in both PPs (Figures 1C–E, S1C) and mLN (Figure S1D) between mice deficient for IgA (*Iga*$^{-/-}$ and co-housed, littermate controls (*Iga*$^{+/+}$), despite an altered distribution of antibody (Ab) isotypes (Figures S1E–J).

However, while PP B cells expressing isotypes other than IgA can effectively become GC B cells, suggesting that IgA is not required for GC formation, it does not rule out a role for the IgA BCR during the GC reaction. GC selection is an iterative immune process controlled by competition among B cell clones[47], thus, we wanted to test whether IgA was required in a competitive setting. To this end, we generated mixed bone marrow (BM) chimeric mice where most B cells (75%) were from *Iga*$^{-/-}$ or *Iga*$^{+/+}$ CD45.2+ donor and the remaining B cells (25%) were from wild-type (WT) CD45.1$^+$ donor (Figure 1F). Flow cytometry analysis revealed that in PPs, *Iga*$^{-/-}$ B cells were largely impaired in their ability to participate in the GC reaction compared to WT B cells, while follicular and GC B cells were present at the same ratio in the control mixed BM chimeras (Figures 1G, 1H). No defect was observed in mLN of either mixed BM chimeras, likely due to the low frequency of IgA$^+$ B cells participating in the GC reaction and their peculiar transforming growth factor-β (TGFβ)-independent[27], commensal-independent[36] nature. The inability of *Iga*$^{-/-}$ B cells to compete in the GC was also apparent in immunohistochemistry staining of PP frozen sections, with CD45.2 *Iga*$^{-/-}$ B cells filling the B cell follicle, while inefficiently entering the GC structure, which was instead dominated by CD45.1 WT B cells. This pattern was reversed in control mixed BM, with CD45.2 *Iga*$^{+/+}$ B cells being more abundant in both B cell follicle and GC (Figure S1K). GC B cells can give rise to both PCs and MemB cells. MemB cells expressing CD73 and CD80 (double positive, DP) are thought to be directly generated in GCs[48]. In line with reduced participation in the GC reaction, mixed BM chimeras revealed that *Iga*$^{-/-}$ B cells also contributed less to GC-derived MemB cells in PPs, but not mLN (Figure 1I). In contrast, IgA deficient B cells were overrepresented in the double-negative (DN, CD73$^-$ CD80$^-$) compartment (Figure 1J), suggesting that IgA is required for optimal GC participation and formation of GC-derived MemB cells.

Chronic GC reactions in PPs and mLN are mainly driven by commensals but can also incorporate responses to pathogens[22,24]. Intestinal inflammation can alter the cytokines milieu and impact GC reaction[49,50]: to test whether intrinsic IgA-deficiency impacts GC

B cell competition upon enteric pathogen encounter, we infected mixed BM chimera with metabolically deficient Salmonella strain (ΔAroA) which is able to induce an IgA response (Figure 1K).[49] Similar to homeostatic conditions, *Iga*$^{-/-}$ B cells were largely outcompeted in the GC of PPs, but enteric infection also preferentially expanded *Iga*$^{+/+}$ B cells over *Iga*$^{-/-}$ B cells in GC reaction in mLN (Figure 1L). In contrast to what was observed during commensal driven responses, DP MemB cells were affected by IgA deficiency in both PPs and mLN upon Salmonella infection (Figure 1M) while DN MemB were largely unchanged (Figure S1L). This discrepancy could be due to enhanced migration of PP-generated DP MemB cells into mLN during Salmonella infection compared to homeostatic situations.

Together our data show that IgA is required for optimal GC persistence and MemB cell formation during both homeostatic responses to commensal bacteria and inflammatory responses driven by pathogenic enteric bacteria.

IgA is required for efficient plasma cell homing to the intestinal lamina propria.

In addition to MemB cells, GC B cells can also differentiate into PCs, and selection during the GC reaction is thought to be critical for the generation of PCs that secrete high affinity Abs[32]. PP GCs generate most IgA-secreting PCs that egress from lymphatics at the basal side of the PPs using S1PR1[51] and home to the lamina propria via the integrin alpha 4 beta 7 (α4β7)[52,53] and C-C chemokine receptor type 9 (CCR9).[54] Administration of the S1PR1 functional antagonist FTY720 traps nascent PCs in the PPs[51], therefore allowing full characterization of PCs before they egress and migrate into the lamina propria. Indeed, the vast majority of PCs expressing α4β7 and CCR9 in PPs were IgA^{+}, while PCs that did not express α4β7 and CCR9 (non-gut-homing) were not enriched as IgA expressing cells in PPs (Figure 2A).

PP-generated PCs egress from efferent lymphatics, that connect to the mLN, on their way to reach the lamina propria: similar to PPs, most α4β7 and CCR9 expressing PCs in mLN were IgA+ (Figure S2A). The requirements for IgA BCR in underpinning gut-tropism is not absolute, as analysis of PCs in FTY720-treated *Iga*$^{-/-}$ mice revealed that IgG1, IgG2b, and IgM B cells were able to upregulate gut-homing receptors (Figure S2B).

In line with this data, absence of IgA does not completely impair gut-homing, as microscopy analysis of fluorescent PCs in the intestinal lamina propria of mice unable to switch to IgA, either because they have selective IgA-deficiency (*Aicda*$^{cre/+}$ *Rosa26*$^{Stop\text{-}tdTomato/+}$ *Iga*$^{-/-}$) Or because they lack the molecular machinery required for class switch recombination (*Aicda*$^{cre/cre}$ *Rosa26*$^{stop\text{-}tdTomato/+}$) did not show decreased PC compartment compared to IgA-sufficient mice (*Aicda*$^{cre/+}$ *Rosa26*$^{stop\text{-}tdTomato/+}$ *Iga*$^{+/+}$) (Figures 2B, 2C, S2C). Analysis of PCs in the lamina propria of *Aicda*$^{cre/+}$ *Rosa26*$^{Stop\text{-}tdTomato/+}$ *Iga*$^{-/-}$ mice revealed that they are mostly IgG2b, with contributions from IgM and IgG1 as well (Figure 2D).

Nevertheless, fully deficient mice might not sufficiently recapitulate physiological aspects of PC biology, as PC generation from GC B cells is dependent on competition-based selection[32]. In mixed chimeras while the total *Iga*$^{-/-}$ PCs were slightly reduced (Figure S2D), a marked reduction was observed in gut-homing *Iga*$^{-/-}$ PCs in both PPs (Figure

2E) and mLN (Figure 2F) while non-gut-homing PCs were minimally altered (Figure 2G, 2H). To determine whether *Iga*$^{-/-}$ PCs were nonetheless able to reach the lamina propria, we generated mixed BM chimeras in which half of PCs , either *Iga*$^{+/+}$ or *Iga*$^{-/-}$, were fluorescently marked (*Aicda*$^{cre/+}$ *Rosa26*$^{stop\text{-}tdTomato/+}$ *Iga*$^{+/+}$ or *Iga*$^{-/-}$) (Figure 2I). While in the *Iga*$^{+/+}$: WT chimera the intestine was repleted with IgA+ PCs, from either WT (non-fluorescent) or *Iga*$^{+/+}$ B cells (tdTom^{+}) (Figures 2J, 2K, S2E), *Iga*$^{-/-}$ PCs (tdTom^{+}) were not observed in the intestine of *Iga*$^{-/-}$: WT chimera, suggesting that IgA-deficiency impairs homing to the LP in a competitive setting (Figures 2J, 2L).

Taken together, these data point to a critical role of surface IgA to instruct the generation of gut-homing PCs. It appears that, while non-IgA expressing B cells can differentiate into PCs, they are largely unable to upregulate homing receptors required for efficient migration into the intestinal lamina propria.

Mixed BM chimeras are a robust experimental system to investigate competitive requirements for immunological processes. However, the need for irradiation can introduce alterations due to cell death, especially in the gut[55]. Therefore, to further expand our findings to a competitive system that does not require irradiation, we took advantage of allelic exclusion, a process by which B cells only transcribe one heavy chain locus during development. As a result of this, IgA heterozygous (*Iga*$^{+/-}$) mice normally develop two genetically distinct sets of B cells, one sufficient for IgA and one deficient for IgA, effectively generating a natural WT:*Iga*$^{-/-}$ chimera (Figure 3A). Since WT and *Iga*$^{-/-}$ cells carry distinct immunoglobulin heavy chain allotypes, allotypic reagents can be used to distinguish B cells from WT (IgH^{b}) and *Iga*$^{-/-}$ (IgH^{a}) origin. Due to allelic exclusion, follicular B cells are present at a 50:50 ratio in both WT (IgH$^{a/b}$) and *Iga*$^{+/-}$ (IgH$^{a/b}$) mice: if surface IgA does not preferentially enhance GC fitness, we expect to observe a 50% reduction of total IgA GC B cells in *Iga*$^{+/-}$ mice compared to WT mice, due to the *Iga*$^{-/-}$ B cells equal contribution to the GC. However, if surface IgA promotes competitiveness in the GC, we anticipate the total IgA GC B cells to be unaffected in *Iga*$^{+/-}$ mice. Indeed, we found that totaI IgA GC B cells were indistinguishable between WT and *Iga*$^{+/-}$ mice, supporting the concept of IgA dominance during GC competition (Figure 3B). In contrast, IgM^{a} B cells (derived from BM that are unable to express IgA) were expanded in activated B cell subsets compared to IgM^{b} WT B cells (Figures 3C, S2F), a finding also observed in mixed BM chimeras (Figure S2G), suggesting that intrinsic IgA deficiency during GC competition allows the persistence of IgM^{+} GC B cells. Allotypic reagents can be used to track the origin of intestinal Ab by staining intestinal content for Ab-coated intestinal bacteria[7,26]: Flow cytometry analysis revealed that the mucosal humoral response was dominated by IgA^{+} cells (Figures 3D, S2H) and unaffected in *Iga*$^{+/-}$ mice, a finding in accordance with the requirement of IgA for intestinal PC generation (Figures 2I, 2K). Intestinal content can also be stained with serum, to measure the circulating Ab response to gut commensals[56]. While no changes were observed in commensal-reactive serum IgA between WT and *Iga*$^{+/-}$ mice (Figure 3E, 3F), *Iga*$^{+/-}$ PCs showed increased contribution to commensal-reactive IgM in serum (Figures 3G, 3H), suggesting that IgA-deficient B cells were able to respond to commensals and differentiate into PCs, but their response was redirected into systemic circulation. To assess whether a similar mechanism was in place during an antigen-specific response to foreign antigen, we orally immunized *Iga*$^{+/-}$, *Iga*$^{-/-}$, and WT mice with cholera

toxin (CT)[57] (Figure 3I). Analysis of Abs from in vitro differentiated MemB cells revealed the anti-CT Ab was dominated by IgA from *Iga*$^{+/+}$ B cells (Figure 3J), while *Iga*$^{-/-}$ B cells increasingly generated anti-CT IgM Abs (Figure 3K) compared to *Iga*$^{+/+}$ B cells (Figure 3L). Together our data support a model where surface IgA BCR allows for efficient participation in the PP GC and PC generation, underpinning efficient humoral immune responses at the intestinal barrier.

Resistance to cell death and T cell help enhance IgA^{+} GC B cell persistence.

The GC is divided into anatomically restricted dark zone (DZ) and light zone (LZ) compartments. While flow cytometry analysis of mixed BM chimeras did not show a preferential reduction of *Iga*$^{-/-}$ B cells in one GC compartment (Figures 4A, 4B, S3A), in situ immunofluorescent microscopy revealed that *Iga*$^{-/-}$ B cells were predominantly clustered in the LZ (Figures 4C, 4D, 4E). The GC reaction couples massive B cell proliferation with carefully controlled cell death to achieve clonal selection. We therefore initially tested the ability of *Iga*$^{-/-}$ B cells to undergo proliferation by measuring BrdU incorporation upon short-term labelling. *Iga*$^{-/-}$ and WT B cells proliferated at similar rates in both GC compartments and in the follicle (Figures 4F, S3B–E). In the DZ, GC B cells undergo cell death in response to the AID-dependent generation of a non-functional BCR.[58,59] To test whether *Iga*$^{-/-}$ B cells were lost at this negative selection stage, we retrovirally expressed *Bcl2*, an anti-apoptotic gene that drives increased B cell survival (Figure S3F) and can rescue defects in DZ GC survival[59] in mixed BM chimeras. Ectopic BCL-2 was unable to rescue *Iga*$^{-/-}$ B cells in both GC and MemB compartments (Figures 4G, S3G), suggesting IgA BCR does not confer competitive advantage during DZ selection.

In the LZ, GC B cells are deleted due to the absence of positive selection, which integrates both BCR signaling and T cell help. Cell death analysis in mixed BM chimera using an antibody against active caspase 3 that identifies apoptotic GC B cells, revealed a higher frequency of apoptosis among LZ, but not DZ, *Iga*$^{-/-}$ B cells (Figures 4H, S3H–I), a phenotype restricted to PPs (Figure S3J). Analysis of *Rosa26*^{INDIA} apoptosis indicator mice which report active caspase 3 via FRET loss[58] also revealed that IgA BCR confers protection from cell death in the LZ during the GC reaction in PPs (Figure 4I). To test whether increased apoptosis resistance in LZ IgA^{+} B cells was associated with higher degree of T cell help, we orally immunized mice with an attenuated Salmonella strain encoding OVA. The same number of GC B cells were sorted according to surface isotypes and co-cultured with naive OVA-specific TCR transgenic CD4^{+} T cells (Figure 4J). In CD4^{+} T cells, CD69 is an early activation marker that is rapidly upregulated upon TCR stimulation by cognate peptide-MHCII complex: IgA^{+} GC B cells induced higher CD69 expression in CD4^{+} T cells compared to IgM^{+} or IgG^{+} GC B cells (Figure 4K). Since no difference was observed in MHCII expression (Figure S3K), our results suggest that IgA expressing GC B cells are either equipped with a more efficient antigen processing and presentation machinery or are better in extracting antigen from follicular dendritic cells. Recently, it has been shown that LZ T cells metabolically refuel LZ GC B cells without controlling their re-entry into S phase[60], a process that can be measured by a short pulse of BrdU. We observed that in the PP LZ, IgA^{+} GC B cells outcompeted other GC isotypes for T cell–derived refueling cues as shown by a higher proportion of IgA^{+} GC B cells had incorporated

BrdU (Figure 4L), with a similar, albeit more subtle, trend also present in mLN (Figure S3L). Correspondingly, using a reporter mouse for c-Myc that can identify GC B cells that received T cell activation signals[61,62], we found that IgA^+ LZ B cells showed increased c-Myc expression, suggesting an integration of stronger positive selection cues (Figure 4M). Together our results support the concept that the IgA BCR protects GC B cells from cell death in the LZ via enhanced T cell-derived positive interaction that permits preferential selection during GC response.

IgA mediates stronger BCR signaling.

In the GC LZ, B cell clones that bind antigen with higher affinity are preferentially selected for survival[58], therefore, we hypothesized that the IgA BCR would mediate stronger BCR signaling. Ex-vivo stimulation of Ca^{2+} dye-loaded GC B cells with pan anti-BCR revealed that, in contrast to IgM^+ or $IgG2b^+$ GC B cells which had undetectable Ca^{2+} responses, as previously reported[37,63], IgA^+ GC B cells spiked calcium readily and consistently (Figures 5A and 5D), a feature also observed using isotype-specific Ab stimulation (Figures 5B and 5E), despite no difference in surface expression of the BCR complex (Figure S4A). To increase sensitivity in BCR-dependent Ca^{2+} release analysis, we also generated mice that express both the red fluorescent protein Tdtomato and the ultrasensitive calcium indicator GCamp6 in GC and post-GC B cells (*Aicda*$^{cre/+}$ *Rosa26*$^{Stop\text{-}tdTomato/gCaMP6}$) and observed a similar IgA-dependent Ca^{2+} release (Figures 5C, 5F, S4B). In contrast, BCR-dependent Ca^{2+} release in MemB cells, albeit faster in IgA^+ cells, was also observed in MemB cells of other isotypes (Figures S4C–S4G), highlighting the difference between GC and MemB cell BCR signaling. The IgA-dependent Ca^{2+} spike was BCR dependent as incubation with Ibrutinib, a BTK inhibitor, reduced the calcium flux observed in both IgA^+ GC and MemB cells (Figures 5F, S4G- S4K) (*22*).

BCR signaling via different isotypes has been shown to mediate various biological outcomes[42,44,45], but little is known about the impact of the IgA BCR on intracellular signaling. Thus, to investigate IgA BCR signaling with increased granularity, we took advantage of CH12 and I29, two unrelated murine B cell lines with the ability to class switch to IgA[64,65], to generate CH12 and I29 as IgM (CH12-M; I29-M) or IgA (CH12-A; I29-A) expressing cell lines (Figures S5A and S5B). Anti-isotype stimulation of CH12 revealed a more profound phosphorylation pattern in CH12-A compared to CH12-M by both western blot and phosphoflow (Figures 5G, 5H, 5I, S5C), including phosphorylation of SYK and BTK (Figures 5J, 5K, S5D). Similar findings were observed in I29 cells (Figures 5L, 5M, S5E).

Both IgA^+ B cell lines were characterized by higher basal phosphorylated protein amounts (Figures 5I, S5F, S5G) which was dependent on the BCR signaling, as treatment with the Syk inhibitor, R406, reduced phosphorylated proteins including pBTK while leaving pSYK unchanged (Figures 5N, 5O, S5H–J). To determine whether IgA BCR mediates stronger BCR signaling in human B cells as well, we stimulated sorted GC from tonsils and observed that IgA^+ GC B cells had increased total phosphorylated proteins compared to IgM^+ GC cells (Figures 5P, 5Q). Our findings highlight that IgA BCR mediates stronger antigen receptor signaling in both basal and activated states, a property also conserved in human.

IgA resistance to FasL-dependent cell death increase GC competitiveness.

In the LZ compartment, in addition to providing help and positively selecting B cells, T cells can eliminate B cells via activation of the FasL-Fas-dependent cell death pathway.[34] Previous reports suggest that different B cell isotypes might be differently sensitive to Fas-mediated killing[66,67], but the role of IgA BCR in this process has not been investigated. Therefore, we sought to test whether IgA BCR confers resistance to Fas-mediated death using CH12 cells, which express similar surface Fas regardless of isotype (Figure S6A), and FasL expressing vesicles, which express the physiological FasL trimer and can induce apoptosis in Fas-expressing cells[68,69]. IgA^+ CH12 were more protected from Fas dependent death compared to IgM^+ CH12, suggesting an IgA intrinsic basal protection, likely driven by tonic, antigen-independent BCR signaling (Figures 6A, S5C).

To test how BCR signaling may offset Fas signaling, CH12 B cells were stimulated immediately prior to incubation with FasL vesicles: while BCR stimulation rescued both CH12-M and CH12-A from Fas-mediated apoptosis, a higher degree of protection was achieved in IgA^+ CH12 (Figure 6B). Conversely, inhibition of BCR signaling with the Syk inhibitor R406 enhanced CH12-M and CH12-A sensitivity to FasL vesicles, with CH12-A showing increased propensity to undergo cell death (Figure 6C). Together this data suggests that IgA BCR signaling provides protection against Fas mediated death initiated by membrane FasL, suggesting an intrinsic mechanism that might underpin IgA GC B cell survival in vivo.

Cell-intrinsic suppression of GC B cell survival via FasL-Fas has been shown to be important in preventing outgrowth of GC; inability to undergo FasL-mediated cell death predisposes the host to autoimmunity and B cell lymphoma.[34,70–72] Such constraints on GC B cell accumulation in vivo is tissue specific: while Fas-dependent deletion is a dominant mechanism to maintain GC in peripheral lymph node and mLN, in PPs, GC B cells resistance to Fas killing did not confer a competitive advantage.[34] In PPs, most GC B cells carry an IgA BCR, thus IgA^+ GC B cells might be equipped with molecular machinery that permits a higher threshold for Fas-dependent cell death. Since GC B cells express similar surface Fas independently from the isotype in PPs, (Figure S6B), we speculated that $Iga^{-/-}$ B cells may be preferentially killed via Fas and therefore could be rescued by inactivation of the Fas-induced cell death pathway. To test this hypothesis, we generated mixed BM chimeras with BM from WT and $Iga^{-/-}$, or *Iga* resistant to Fas-mediated cell death ($Iga^{-/-}$ $Fas^{lPr/lpr}$). In PPs, we observed that, in contrast to $Iga^{-/-}$ B cells, $Iga^{-/-}$ $Fas^{lpr/lpr}$ B cells were able to compete with WT B cells during GC reaction in both LZ and DZ (Figures 6D, 6E), and their restored GC fitness led to physiologic MemB cell compartment formation (Figure 6F). In mLN, where a very small number of GC B cells express IgA BCR, resistance to Fas-mediated cell death allowed $Iga^{-/-}$ $Fas^{lpr/lpr}$ B cells outgrowth as GC B cells and MemB cells, supporting previous findings[34] (Figures S6C, S6D). No preferential isotype expansion was observed in $Iga^{-/-}$ $Fas^{lpr/lpr}$ B cell subsets (Figures S6E, S6F), suggesting that the GC competitive ability was not driven by B cells carrying a specific isotype, but was instead the result of global rescue of GC B cells from Fas-mediated cell death. Finally, although $Iga^{-/-}$ $Fas^{lpr/lpr}$ GC B cells could generate PCs at a rate similar to WT B cells (Figure S6G) they were nevertheless unable to differentiate into gut-homing PCs (Figures 6G, 6H) highlighting

a previously undescribed role for the IgA BCR in mucosal imprinting that is uncoupled from GC selection. In line with this finding, mixed BM chimeras generated in μMT hosts using allotypic donors (IgH^a vs IgH^b) to track Ab origins revealed that endogenous intestinal bacteria were coated with IgA coming from WT B cells (Figure 6I), with negligible contribution of IgM from $Iga^{-/-}$ $Fas^{lpr/lpr}$ (Figure S6H). In contrast, Iga^{--} $Fas^{lpr/lpr}$ serum gave rise to more IgM specific to commensals (Figure 6J), likely due to B cell outgrowth in mLN (Figures S6C, S6F). These results indicate that Fas counterselection is critical for IgA^+ GC B cells' enhanced competition and point to an IgA-intrinsic resistance to Fas-dependent cell death in vivo. However, rescue of non-IgA GC B cells by Fas deletion does not increase the generation of gut-homing PCs , suggesting that additional mechanisms in IgA GC B cells imprint the ability to direct PCs to the intestinal mucosa.

Discussion

Acquisition of surface IgA upon IgA class switch recombination is routinely described as a default B cell differentiation outcome driven by the abundant active TGFβ available in PP sub-epithelial dome to recently activated B cells.[26,27] This process imprints the B cell response to intestinal antigen for the generation of mostly IgA-secreting PCs. The incorporation of J-chain for rapid retrotranslocation via pIgR[73,74], the dimeric form for increased avidity[75], and the somatic mutation loads[16–20] render IgA the most efficient mucosal antibody isotype. Thus, induction of the IgA response was mainly viewed simply as a process geared toward the generation of essential antibodies for intestinal secretion.

Here we described a role of IgA during the GC B cell reaction, providing an additional perspective on the evolutionary requirements of IgA class switch in B cells. IgA is critical both to promote fitness during the GC reaction and to imprint gut-homing properties on nascent PCs. The conflicting demands of broad IgA reactivity and affinity-based GC selection has been partially reconciled by recent works describing tunable affinity maturation in Peyer's patches[35,36], but the mechanism underpinning the GC reaction to intestinal antigens have not been elucidated. Lower microbiome complexity that restores affinity maturation efficiency and leads to enhanced clonal selection in PP GC is associated with reduced IgA^+ GC B cells[36], suggesting IgA BCR tunes GC selection toward a more permissive reactivity. How, then, are IgA^+ B cells selected during the GC reaction to generate a humoral intestinal response that can simultaneously coat several classes of commensals? We propose a model in which the IgA BCR is inherently required for the generation of the broad mucosal antibody repertoire. IgA^+ GC B cells display intrinsic protection from apoptosis that is centered around an enhanced BCR intracellular signaling and increased T cell-derived positive cues during selection of antigen-specific clones. Mechanistically, IgA BCR allows GC B cells to offset the Fas-FasL cell death signaling, therefore allowing low affinity B cells to persist and contribute to the PC compartment. While our paper was in revision, a manuscript was published detailing how BCR signaling in non-intestinal GC contributes to the selection of high-affinity clones into the PC pool[76]. These findings dovetail well with our model, with higher IgA BCR signaling preferentially selecting IgA^+ B cell clones for participation to the intestinal humoral response.

The structural basis for the superior positive selection of IgA GC B cells remains unclear. While reports exist that the intracellular tail of IgG1 and IgE do not contribute to their intrinsic effect on GC positive selection, the IgA intracellular tail is distinct from all the other isotypes both in terms of length and sequence and could underpin the specific effect on IgA^+ GC B cells during responses in PPs. Additionally, it also conceivable that Ig isotype-specific membrane and constant regions could play a role in IgA expressing cells, by either facilitating BCR clustering and thus lowering the threshold of B cell selection in the GC, or by altering BCR stiffness and thus rendering IgA+ GC B cells superior in extracting antigen displayed on Follicular dendritic cells.[77,78]

While in our model strong IgA BCR signaling promotes GC competition, IgE BCR mediates autonomous, sustained calcium signaling which constrains GC formation and promotes PC differentiation.[42,45] Fas deletion increases IgA-deficient cells competitiveness in PP GC reaction, while Fas-deficient B cells generate a high number of IgE+ PC in periphery.[72] One possible explanation for these apparently contradicting results is that BCR signaling is graded in GC B cells carrying different isotype: IgE strongest signaling promotes PC formation in line with a strength of signaling model[31,79], while IgA BCR signaling, while dominant over the other BCR isotypes present in PP GC, allows for both GC competition and PC differentiation. IgE B cells do not efficiently participate in the GC reaction and it is unlikely that they are sensitive to FasL-induced death at that stage. Thus, the high IgE titer observed in the Fas or FasL deficient mice might be due to expansion of $IgG1^+$ GC B cells that sequentially switch to IgE and then contribute to the humoral immunity. The stricter FasL-mediated counterselection of low affinity non-IgA GC B cells is an appropriate strategy to avoid the generation of rogue, autoreactive B cell clones[34,72]

Our results indicate a preferential effect of IgA BCR in PP GC competition compared to mLN and data exist supporting different requirements for IgA GC B cells at these two sites, including dependency on TGFβ signaling for IgA CSR[27], on Gα13-coupled receptors for GC formation[80,81], on Fas for GC counterselection[34], and on commensals for GC response[77]. Two non-mutually exclusive hypotheses could explain the observed difference between IgA GC in PP and mLN. mLN IgA+ GC B cells could be responding against self-antigen or retroelements and have such low initial affinity that IgA-mediated enhanced BCR signaling only allows for their survival, not for the acquisition of competitive advantage. Additionally, mLN could contain specific environmental factor(s) that modulate GC selection in mLN in a distinct fashion compared to PPs, therefore muting IgA-dependent effect in competition. Additional investigations are required into the nature and origin of IgA^+ GC in mLN to mechanistically tease apart their distinct regulation compared to IgA+ GC in PPs.

We also discovered that the IgA BCR was required in a competitive setting for the efficient upregulation of migratory receptors CCR9 and α4β7 and homing of intestinal PCs. This process is independent of Fas-FasL, as restoring competitiveness of non-IgA B cells during GC reaction had no effect on their ability to upregulate CCR9 and α4β7. Thus, additional step(s) that control functional generation of intestinal humoral immunity must take place in PPs during the response to intestinal antigen. While the homing ability could be imprinted during LZ selection in the GC, it is not possible to rule out that BCR signaling could

shape PC homing outside of the GC reaction.[82,83] IgA PCs isolated from lungs and mediastinal lymph nodes of mice infected with influenza also show marked upregulation of mucosal homing receptors[84], suggesting a direct link between IgA BCR and PC migratory capabilities that is independent of the niche that generates PCs. Future investigations will be required to elucidate the cellular and environmental components that which signals, and at which step of PC differentiation, contribute to acquisition of gut tropism in IgA^+ B cells. Moreover, whether this process remains in place or is altered during enteric infection or dysbiosis, states that can lead to non-IgA PC homing to the lamina propria,[85–87] will require additional studies.

Given the dynamic impact of IgA on gut autoinflammation and enteric infection, understanding how IgA B cells are selected in the GC and give rise to IgA intestinal responses could be exploited therapeutically to develop strategies that restore commensal homeostasis or enhance mucosal vaccine responses.

Limitations of the study

Our data indicate that IgA BCR endows GC B cells with enhanced competitive capacity by offsetting FasL counterselection. In spleen, FasL counterselection removes low affinity GC B cell clones: while we speculated that IgA BCR allows commensal-reactive low affinity clones to persist and to participate in the intestinal humoral response, we have not formally proven it. A high resolution, more comprehensive chart of GC B cell antigen-receptors and the corresponding commensal antigens coupled with direct biophysical affinity measurements will be needed to evaluate the impact of IgA BCR on commensal-reactive GC reaction. Moreover, our ex-vivo and in vitro data suggest that IgA BCR mediates stronger BCR signaling compared to other isotypes in the PP GC. However, in vitro stimulation might not recapitulate the antigen nature, stiffness, and mode of presentation during GC reaction in vivo. In vivo stimulation with physiologic commensal-derived antigens will be needed to carefully evaluate isotype-specific BCR signaling in GC B cell during intestinal humoral response.

STAR METHODS

RESOURCE AVAILABILIY

Lead contact—Additional information and requests for resources and reagents should be directed to and fulfilled by the lead contact, Andrea Reboldi (andrea.reboldi@umassmed.edu).

Materials Availability—Reagents, plasmids, and mouse lines reported in this study are available upon signing a Materials Transfer Agreement.

Data and code availability—No original code has been reported in this paper.

EXPERIMENTAL MODELS AND SUBJECT DETAILS

Mice—All mice at UMass Chan Medical School were group housed (up to 5 mice of the same sex) and maintained under standard 12:12 hours light/dark conditions and housed

in specific pathogen-free (SPF) conditions. Female and male mice were analyzed at 8-12 weeks of age and littermates of the same sex were cohoused and randomly assigned to groups. CD45.2, CD45.1, R26^{tdTomato}, Aicda^{cre}, Fas^{lpr}, gCAMP^{gfp}, OT II, and μMT were purchased from the Jackson Laboratory. Gregory Barton provided *Iga*$^{-/-}$ mice, IgM^{a} mice were from an internal colony. C.T.M. provided Rosa26^{INDIA} mice.[58] O.B. provided cMYC-GFP mice. All procedures were conformed to ethical principles and guidelines approved by the UMass Chan Medical School Institutional Animal Care and Use Committee.

METHOD DETAILS

Bone marrow chimeras, retroviral transduction—CD45.1/2, WT, or μMT mice were lethally irradiated twice with 550 rads gamma-irradiation, 3 hours apart, then intravenously injected with 1-3 x 10^6 bone marrow cells. Bone marrow was harvested by flushing both tibia and femurs of donor mice, counted, and mixed at ratios indicated in text. Mice were analyzed 8-12 weeks after cell transfer.

For retroviral transduction, PlatE cells were transfected with murine stem cell virus retroviral constructs encoding full length Bcl2 with Lipofectamine 2000 following manufacturer's protocol. For transduction of BM-derived cells, BM was harvested 4 days after 5-flurouracil injection and cultured in the presence of recombinant IL-3 (20 ug/ml), IL-6 (50ug/ml), and mouse stem cell factor (100 ng/ml). BM cells were spin-infected twice with a retroviral construct expressing Bcl2 with GFP as a reporter. One day after the last spin infection, the cells were injected into lethally irradiated CD45.1/2 recipients. Mice were analyzed 8-10 weeks later.

In vivo treatment, immunization, and infection models—To prevent lymphocyte egress from Peyer's patches (PPs), the S1PR1 agonist FTY-720 was dissolved in saline solution and administered to mice daily i.p. at 1 mg/kg for 7 days.

For cholera toxin responses, mice were immunized with 10 ug of cholera toxin in PBS by oral gavage. Animals received cholera toxin every 7 days for three consecutive weeks. Memory B cells were sorted and analyzed 7 days after last immunization.

The SL1344 metabolically defective (ΔAroA) S. typhimurium strains were provided by Milena Bogunovic (UMass Chan) and grown at 37°C in Luria broth supplemented with appropriate antibiotics to preserve mutation and plasmid. To induce Ova expression, IPTG was added at an OD_{600} of 0.4 and allowed to grow for another 2 hours. For the Salmonella infection, wildtype mice were orally gavage three times, on alternate days with 10^9 CFUs of ΔAroA Salmonella in 200 uL 5% sodium bicarbonate.

For antigen presentation experiments, 3 days after the last dose, follicular and germinal center B cells were sorted from PPs. For mixed BM chimera infections, 8 weeks after BM reconstitution, mice were infected as described above. Seven days after the third dose of Salmonella, mice were scarified, and B cell populations were assessed by flow cytometry.

Sample Preparation and Flow Cytometry—PPs and mesenteric lymph nodes (mLN) were collected into complete media (RPMI, 5% heat inactivated FCS, 10 mM HEPES,

1% Pen/Strep). The tissue was then smashed through a 70 micron cell strainer. Isolated cells were then washed with FACS buffer (DPBS, 2% heat inactivated FCS, 2mM EDTA). Cell suspensions were stained with LIVE/DEAD Fixable Aqua Dead Cell Stain or Fixable Viability Dye eFluor780 in FACS buffer, and Fc receptors blocked with anti-mouse CD16/32. BD Cytofix/Cytoperm kit was used for fixation and intracellular staining. Cells were incubated for 20 min on ice with antibodies described in Key Resource Table. Data were collected on a BD SORP or LSR II and analyzed in FlowJo v10 software.

Lamina propria (LP) lymphocytes were isolated as previously described.[29,88] Briefly, the small intestine was dissected and flushed with cold PBS and PPs removed. The small intestine was divided into 2 equal parts, opened longitudinally and vortexed in a 50 ml conical tube containing HBSS supplemented with 5% heat-inactivated FBS and 10mM HEPES. Epithelial cells were removed by rotating the tissue in RPMI medium supplemented with 5% heat-inactivated FCS, 10mM HEPES, 10mM EDTA for 30 minutes at 37°C. The intestinal pieces were then washed with complete media (RPMI supplemented with 10% heat-inactivated FCS, 10 mM HEPES, 1% P/S), chopped with scissors, and digested at 37°C for 30 minutes in digestion media (complete media supplemented with 0.5 mg/ml Collagenase type IV and 50 ug/ml DNase I). Digested tissue was passed through 70 micron cell strainer and isolated cells were resuspended in 40% Percoll-RPMI and layered with 80% Percoll-RPMI and subsequently centrifuged for 20 min at 2200 RPM with the break off. The isolated LP cells were then stained for flow cytometry analysis as described above.

For anti–active caspase-3 staining, cells were maintained on ice during harvesting and processing. Cells were stained for with biotin–conjugated anti–active caspase-3 following fixation and permeabilization according to the manufacturer's instructions and subsequently stained with FITC or AF647 streptavidin.

Bacterial flow cytometry was performed as previously described.[56] Briefly, bacteria were washed in sterile-filtered DPBS with 1% BSA and resuspended at approximately 5 x 10^6 bacteria/mL. Mouse serum was diluted 1:25 in PBS/BSA buffer and 25 uL of this solution was mixed with 25 uL diluted microbes in u-bottom plate. Staining was performed with purified or fluorochrome conjugated antibodies. Cells were washed and resuspended in 1% BSA in DPBS with SYBR Green and analyzed by flow cytometry.

Cell sorting—For sorting, cells were stained as described above and sorted on a BD FACSAria II with an 85 micron nozzle. Cells were maintained at 4°C until sorting. Sorted PP Follicular and germinal center B cells were used for antigen presentation. PP memory B cells were used for NB21 co-culture. Germinal center B cells were sorted as live IgD^- $GL7^+$ $CD38^-$ $CD138^-$ $isotype^+$, Follicular as live IgD^+ $GL7^-$ $CD138^-$, and memory B cells as live IgD^- $GL7^+$ $CD38^+$ $CD138^-$ $CD73^+$ $CD80^+$ respectively into complete media for further culture.

BRDU

For BrdU incorporation experiments, animals were given 2.5 mg of BrdU in a single i.p. injection and sacrificed 30 minutes or 3.5 hours later. Staining was performed using the FITC BrdU Flow Kit according to the manufacturer's instructions. To stain for intracellular

antigens, cells were first stained for surface markers and then fixed and permeabilized using the BD Cytofix/Cytoperm Kit per the manufacturer's instructions.

Cell line culture conditions—Both CH12 and I29 were cultured in B cell media (10% FCS, 100 units/mL penicillin, 100 units/mL streptomycin, MEM nonessential amino acids, 10mM HEPES, 1mM sodium pyruvate, 55mM 2-Mercaptoethanol). To induce class switch to IgA, CH12 and I29 cells were cultured for 48 hours with 2ng/ml TGFβ and 50 ug/ml LPS. The IgA^+ or IgM^+ population was sorted with a BD FACS Aria II and maintained as CH12 expressing IgM or IgA cell lines and I29 expressing IgM or IgA cell lines.

memB NB21 co-culture—Freshly isolated memory B cells from PPs were FACS sorted as described above and cocultured with NB21 feeder cells as previously described with adjustments.[59,89] Briefly 15,000 NB21.2D9 cells/well were seeded into 96-well u bottom plates in 100 uL of B cell media and grown at 37°C and 5% CO_2 the morning of B cell sorting and coculturing (Day 0). 2000 memory B cells in 100 uL B cell media were added to each well. Culture plates were centrifuged at day 3.5 and the supernatant collected for antibody detection.

FasL vesicle preparation and killing assay—FasL vesicles were prepared as previously described.[90] Briefly, FasL vesicles were collected from N2-mFasL cells that overexpress mouse FasL and empty vesicles from Neo-N2 cells that did not contain FasL used as control. When cells reached ~70% confluence, fresh culture medium without G418 replaced the G418-containing medium. 48 hours later, the supernatants were collected and centrifuged at 4°C, 13,000 rpm in a Sorvall Superspeed centrifuge for 30 min to remove cell debris. Next, the cell-free supernatants were centrifuged for 3 hours at 4°C at 25,000 rpm in a Beckman ultracentrifuge with a SW25 rotor. Following ultracentrifugation, the murine FasL vesicle pellet was suspended with culture medium to 7% of the original volume and passed through a 0.45 micron sterile filter and used for cytotoxicity assays.

For the in vitro FasL killing, 200,000 CH12 cells were plated in 50 uL of warmed calcium media in u-bottom 96 well plates. FasL or empty vesicles were diluted in warm calcium media (DMEM with 2.5% FCS and 10mM HEPES) at the dilutions indicated in the figures and 50 uL were added to each well. Cells were incubated at 37°C with 5% CO2 for 5 hours. Cell death was assessed with annexin V and DAPI. For annexin V staining, cells were stained according to the manufacturer's instructions. DAPI was added after annexin V staining right before cells were collected by flow cytometry. In R406 and FasL killing assays, CH12 were treated with for 18 hours (overnight) with 1.85uM R406 or DMSO. The next morning, cells were washed and resuspended in new calcium media containing 1.85uM R406 or DMSO and FasL vesicles.

Calcium flux assay—For calcium stimulation, PPs were harvested into warm calcium media (DMEM with 2.5% FCS and 10mM HEPES) and processed as described above. Germinal center and memory B cells were enriched for using EasySept negative B cell enrichment with modifications. Briefly, PPs were incubated with biotinylated antibodies against IgD, CD3, CD4, CD8, and CD138. Following negative enrichment, experiments using calcium dyes were incubated with surface antibodies GL7 and CD38 and 6uM

FuraRed and 3uM Fluo-3 AM at 37°C for 20 minutes. Cells were washed and resuspended in warmed calcium media and rested 15 minutes at 37°C prior to stimulation. For gCAMP experiments, after negative B cell enrichment, cells were stained with GL7 and CD38 at room temperature for 10 minutes, washed and rested at 37°C for 15 minutes before stimulation. In some experiments cells were incubated with 100 nM Ibrutinib for 10 minutes at room temperature after surface staining. For all calcium experiments, the first 30 seconds were collected as baseline before cells were stimulated with either individual anti-BCR at 10 ug/mL or pan anti-BCR (10 ug/ml each of goat anti-mouse IgM, IgA, and IgG2b mixed). After 2-3 minutes 1ug/mL Ionomycin was added to measure maximum calcium flux.

Cell line BCR stimulation—For CH12 and I29 BCR stimulation, 200,000 B cells were resuspended in 400 ul of warm calcium media and rested for 30 minutes prior to stimulation. Cells were stimulated with 10ug/mL anti-BCR in warm calcium media for 1 minute then fixed for western blot or phospho-flow. For western blots, cells were spun at max speed room temperature for 10 seconds, the supernatant was removed, and the cell pellet was lysed in RIPA buffer with phosphatase inhibitor. Lysed cells were left on ice for 30 minutes then spun down at max speed for 10 minutes. The supernatant was used as whole cell lysates for western blots. Whole cell lysates were boiled for 5 minutes in Laemmli sample buffer and 2-ME then run on a 10% tris-glycine gel. Proteins were transferred to polyvinylidene fluoride membrane and blocked with 2% BSA in TBS-Tween for one hour at room temperature then incubated with anti-mouse phosphotyrosine-HRP antibody overnight at 4°C. Blots were washed with TBST followed by development with SuperSignal West Pico PLUS chemiluminescent Substate. Actin was detected with mouse anti-actin for 1.5 hours at room temperature followed by anti-mouse HRP for 1.5 hours and detected with ECL Prime Western blotting detection reagent. ImageJ software was used for band densitometry.

For phosphoflow, after anti-BCR stimulation, cells were fixed with 16% PFA at a final concentration of 1% PFA for 10 minutes room temperature. Cells were pelleted and resuspended in 1 mL of ice-cold methanol and left overnight at −20°C. The following day, cells were washed with 3 ml of FACS buffer and then 4 ml of FACS buffer. Cells were blocked in a u-bottom 96 well plate for 20 minutes with Fc block at room temperature, then stained with phosphor-tyrosine or phosphoBTK antibodies for 45 minutes at room temperature and then analyzed by BD SORP or LSR II.

For Syk inhibition, 200,000 I29 or CH12 cells were incubated at 37°C in calcium media containing 2uM R406 Syk inhibitor for 45 minutes. Cells were washed with warm calcium media and pelleted. Cells were resuspended in warm calcium media and immediately fixed for phosphoflow as described above.

In vitro antigen presentation—For antigen presentation assays, follicular, IgM+, IgG+ and IgA+ germinal center B cells were sorted from PPs as described above. OT-II T cells were isolated from spleens of OT-II Rag KO mice. B cells and T cells were co-cultured 1:1 in 200 uL of B cell media in 96 well u-bottom tissue culture plate and incubated at 37°C for 18 hours. CD69 expression on OT-II T cells was assessed by flow cytometry.

Immunohistochemistry and Immunofluorescence—For immunohistochemistry, acetone fixed cryosections were stained goat purified anti-mouse IgD and biotin anti mouse GL7. Then sections were stained with the secondary antibodies anti-goat HRP and streptavidin AP. HRP and AP were developed using DAB reagents and Fastblue (2mg/ml).

For immunofluorescence, tissues were fixed in 4% paraformaldehyde in phosphate buffer overnight at 4°C, washed three times for 30 min in PB, then moved to 30% sucrose in PB overnight. Tissues were flash frozen in cryomolds and the next day, 7 micron sections were cut and then dried for at least 1 hour before staining. Sections were rehydrated in PBS with 1% BSA for 10 min and then stained overnight at 4°C and stained for subsequent steps at room temperature for two hours, all in PBS with 1% BSA, 2% mouse serum, 2% rat serum, and 2% donkey serum. PP sections were stained with primary antibodies: Goat anti-mouse IgD, rabbit anti-mouse RFP, and Alexa647-conjugated anti-CD35/21. Sections were then stained with the secondary antibodies: Cy3 anti-rabbit, AF488 anti-goat, and DAPI. tdTomato cells were counted in the LZ ($CD35^+$) and DZ ($CD35^-$) regions using ImageJ.

Small intestinal villi were first stained with directly conjugated goat anti-mouse IgA FITC and rabbit anti-mouse RFP and subsequently stained with Cy3 anti-rabbit. $tdTom^+$ cells were quantified in both duodenum and ileum villi.

Human tonsils preparation and stimulation—Human tonsil cells were thawed in 37°C IMDM media with 10% Fetal Bovine Serum (FBS), 1% Glutamax, 1% HEPES, 1% Penicillin/Streptomycin and 0.1% 2-Mercaptoethanol. Single cell suspensions were blocked with Fc Block at 4°C for 10min and subsequently, stained with antibodies to identify Germinal Center B cell and Follicular B cells. For sorting of IgA^+ GC B cells without stimulating the desired population, cells were incubated IgG FITC and IgM PE, and the double negative population was sorted with FACS Aria. For sorting of IgM^+ GC B cells without stimulating the desired population, cells were labeled with additional IgG FITC and IgA PE and sorted as above.

For the western blot signaling assay, sorted cells were rested and stimulated with 10ug/ml anti-IgA or anti-IgM for 5 min. Cells were lysed for 30 min on ice in RIPA buffer containing 0.5% dithiothreitol (DTT) and protease inhibitor cocktail. Lysates were centrifuged for 10 min at 4°C at 14,000g and supernatant was collected. Proteins were separated by electrophoresis using NuPage-Bis-Tris gels and blotted onto polyvinylidene fluoride membranes. Non-specific binding was blocked with 5% BSA in 0.1% TBS-Tween followed by incubation with anti-phosphotyrosine overnight at 4 °C and secondary antibody HRP conjugated antibodies for 1 hour at room temperature. Membranes were washed thoroughly with 0.1% TBS-Tween after antibody incubations and developed using ECL reagents. For re-probing, blots were stripped for 10 min at room temperature with Restore PLUS stripping buffer. Blots were then incubated with β-actin primary antibody and secondary antibody HRP-conjugated antibody for 1 hr at room temperature, washed with TBS-Tween, and developed using ECL reagents. ImageJ software was used for band densitometry.

Statistical analysis and reproducibility—Statistical analyses were performed using GraphPad Prism v10.0 using two-way ANOVA with Bonferroni's multiple comparisons test or unpaired two tailed Student's t test. Data are presented as means ± SEM except Figure 3B and 3C are SD. Differences between group means were considered significant at indicated p value. The significance values are stated in all graphs and the number of biological replicates (n) is stated in the figure legends.

Supplementary Material

Refer to Web version on PubMed Central for supplementary material.

ACKNOWLEDGMENTS

We thank Carol Schrader for the I29μ cell line, Stephanie Moses for FasL vesicle preparation, Garnett Kelsoe for generously allowing use of NB21 cells, and Kelsey Howley and Carly Burke for mouse genotyping and colony maintenance. We thank E. V. Dang for critical reading of the manuscript.

This work was supported by National Institutes of Health (NIH) grant AI155727 and AI173903 (to A.R.), AI151167 (to M.A.) and NIH training grants AI132152 and AI007349 (to F.R.). J.R.M. is supported by the Intramural Research Program of the National Institutes of Health, Center for Cancer Research, National Cancer Institute.

INCLUSION AND DIVERSITY

We support inclusive, diverse, and equitable conduct of research.

REFERENCES

1. Catanzaro JR, Strauss JD, Bielecka A, Porto AF, Lobo FM, Urban A, Schofield WB, and Palm NW (2019). IgA-deficient humans exhibit gut microbiota dysbiosis despite secretion of compensatory IgM. Scientific Reports 9, 1–10. 10.1038/s41598-019-49923-2. [PubMed: 30626917]
2. Fadlallah J, El-Kafsi H, Sterlin D, Juste C, Parizot C, Dorgham K, Autaa G, Gouas D, Almeida M, Lepage P, et al. (2018). Microbial ecology perturbation in human IgA deficiency. Science Translational Medicine 10, eaan1217. 10.1126/scitranslmed.aan1217. [PubMed: 29720448]
3. Suzuki K, Meek B, Doi Y, Muramatsu M, Chiba T, Honjo T, and Fagarasan S (2004). Aberrant expansion of segmented filamentous bacteria in IgA-deficient gut. P Natl Acad Sci Usa 101, 1981–1986. 10.1073/pnas.0307317101.
4. Hand TW, and Reboldi A (2021). Production and Function of Immunoglobulin A. Annu. Rev. Immunol 39, 695–718. 10.1146/annurev-immunol-102119-074236. [PubMed: 33646857]
5. Savilahti E, Klemola T, Carlsson B, Mellander L, Stenvik M, and Hovi T (1988). Inadequacy of musocal IgM antibodies in selective IgA deficiency: Excretion of attenuated polio viruses is prolonged. J Clin Immunol 8, 89–94. 10.1007/bf00917895. [PubMed: 2836474]
6. Bunker JJ, Erickson SA, Flynn TM, Henry C, Koval JC, Meisel M, Jabri B, Antonopoulos DA, Wilson PC, and Bendelac A (2017). Natural polyreactive IgA antibodies coat the intestinal microbiota. Science 358, eaan6619–20. 10.1126/science.aan6619. [PubMed: 28971969]
7. Palm NW, Zoete M.R. de, Cullen TW, Barry NA, Stefanowski J, Hao L, Degnan PH, Hu J, Peter I, Zhang W, et al. (2014). Immunoglobulin A Coating Identifies Colitogenic Bacteria in Inflammatory Bowel Disease. Cell 158, 1000–1010. 10.1016/j.cell.2014.08.006. [PubMed: 25171403]
8. Rollenske T, Szijarto V, Lukasiewicz J, Guachalla LM, Stojkovic K, Hartl K, Stulik L, Kocher S, Lasitschka F, Al-Saeedi M, et al. (2018). Cross-specificity of protective human antibodies against Klebsiella pneumoniae LPS O-antigen. Nat Immunol 19, 1–15. 10.1038/s41590-018-0106-2.

9. Sterlin D, Fadlallah J, Adams O, Fieschi C, Parizot C, Dorgham K, Rajkumar A, Autaa G, El-Kafsi H, Charuel J-L, et al. (2019). Human IgA binds a diverse array of commensal bacteria. J Exp Med 217, e20181635. 10.1084/jem.20181635.
10. Pabst O, and Slack E (2019). IgA and the intestinal microbiota: the importance of being specific. Mucosal Immunol 13, 1–10. 10.1038/s41385-019-0227-4. [PubMed: 31719642]
11. Yang C, Chen-Liaw A, Spindler MP, Tortorella D, Moran TM, Cerutti A, and Faith JJ (2022). Immunoglobulin A antibody composition is sculpted to bind the self gut microbiome. Sci Immunol 7, eabg3208. 10.1126/sciimmunol.abg3208. [PubMed: 35857580]
12. Tezuka H, Abe Y, Asano J, Sato T, Liu J, Iwata M, and Ohteki T (2011). Prominent Role for Plasmacytoid Dendritic Cells in Mucosal T Cell-Independent IgA Induction. Immunity 34, 247–257. 10.1016/j.immuni.2011.02.002. [PubMed: 21333555]
13. Bunker JJ, Flynn TM, Koval JC, Shaw DG, Meisel M, McDonald BD, Ishizuka IE, Dent AL, Wilson PC, Jabri B, et al. (2015). Innate and Adaptive Humoral Responses Coat Distinct Commensal Bacteria with Immunoglobulin A. Immunity 43, 1–14. 10.1016/j.immuni.2015.08.007. [PubMed: 26200004]
14. Grasset EK, Chomy A, Casas-Recasens S, Gutzeit C, Bongers G, Thomsen I, Chen L, He Z, Matthews DB, Oropallo MA, et al. (2020). Gut T cell–independent IgA responses to commensal bacteria require engagement of the TACI receptor on B cells. Sci Immunol 5, eaat7117. 10.1126/sciimmunol.aat7117. [PubMed: 32737068]
15. Kawamoto S, Maruya M, Kato LM, Suda W, Atarashi K, Doi Y, Tsutsui Y, Qin H, Honda K, Okada T, et al. (2014). Foxp3+ T Cells Regulate Immunoglobulin A Selection and Facilitate Diversification of Bacterial Species Responsible for Immune Homeostasis. Immunity 41, 152–165. 10.1016/j.immuni.2014.05.016. [PubMed: 25017466]
16. Dunn-Walters DK, Boursier L, and Spencer J (1997). Hypermutation, diversity and dissemination of human intestinal lamina propria plasma cells. Eur. J. Immunol 27, 2959–2964. 10.1002/eji.1830271131. [PubMed: 9394824]
17. Fischer M, and Küppers R (1998). Human IgA- and IgM-secreting intestinal plasma cells carry heavily mutated VH region genes. Eur. J. Immunol 28, 2971–2977. 10.1002/(sici)1521-4141(199809)28:09<2971::aid-immu2971>3.0.co;2-3. [PubMed: 9754584]
18. Barone F, Vossenkamper A, Boursier L, Su W, Watson A, John S, Walters DKD, Fields P, Wijetilleka S, Edgeworth JD, et al. (2011). IgA-Producing Plasma Cells Originate From Germinal Centers That Are Induced by B-Cell Receptor Engagement in Humans. YGAST 140, 947–956. 10.1053/j.gastro.2010.12.005.
19. Kabbert J, Benckert J, Rollenske T, Hitch TCA, Clavel T, Cerovic V, Wardemann H, and Pabst O (2020). High microbiota reactivity of adult human intestinal IgA requires somatic mutations. Journal of Experimental Medicine 217, 612–613. 10.1084/jem.20200275.
20. Benckert J, Schmolka N, Kreschel C, Zoller MJ, Sturm A, Wiedenmann B, and Wardemann H (2011). The majority of intestinal IgA+ and IgG+ plasmablasts in the human gut are antigen-specific. J. Clin. Invest 121, 1946–1955. 10.1172/jci44447. [PubMed: 21490392]
21. Wei M, Shinkura R, Doi Y, Maruya M, Fagarasan S, and Honjo T (2011). Mice carrying a knock-in mutation of Aicda resulting in a defect in somatic hypermutation have impaired gut homeostasis and compromised mucosal defense. Nat Immunol 12, 264–270. 10.1038/ni.1991. [PubMed: 21258321]
22. Reboldi A, and Cyster JG (2016). Peyer's patches: organizing B-cell responses at the intestinal frontier. Immunological Reviews 271, 230–245. 10.111l/imr.12400. [PubMed: 27088918]
23. Gibbons DL, and Spencer J (2011). Mouse and human intestinal immunity: same ballpark, different players; different rules, same score. Mucosal Immunol 4, 148–157. 10.1038/mi.2010.85. [PubMed: 21228770]
24. Weinstein PD, and Cebra JJ (1991). The preference for switching to IgA expression by Peyer's patch germinal center B cells is likely due to the intrinsic influence of their microenvironment. J Immunol 147, 4126–4135. [PubMed: 1753088]
25. Craig SW, and Cebra JJ (1971). PEYER'S PATCHES: AN ENRICHED SOURCE OF PRECURSORS FOR IGA-PRODUCING IMMUNOCYTES IN THE RABBIT. Journal of Experimental Medicine 134, 188–200. 10.1084/jem.134.1.188. [PubMed: 4934147]

26. Reboldi A, Arnon TI, Rodda LB, Atakilit A, Sheppard D, and Cyster JG (2016). IgA production requires B cell interaction with subepithelial dendritic cells in Peyers patches. Science 352, aaf4822–aaf4822. 10.1126/science.aaf4822. [PubMed: 27174992]
27. Albright AR, Kabat J, Li M, Raso F, Reboldi A, and Muppidi JR (2019). TGFβ signaling in germinal center B cells promotes the transition from light zone to dark zone. J Exp Med 216, 2531–2545. 10.1084/jem.20181868. [PubMed: 31506281]
28. Roco JA, Mesin L, Binder SC, Nefzger C, Gonzalez-Figueroa P, Canete PF, Ellyard J, Shen Q, Robert PA, Cappello J, et al. (2019). Class-Switch Recombination Occurs Infrequently in Germinal Centers. Immunity 51, 1–37. 10.1016/j.immuni.2019.07.001. [PubMed: 31315028]
29. Trindade BC, Ceglia S, Berthelette A, Raso F, Howley K, Muppidi JR, and Reboldi A (2021). The cholesterol metabolite 25-hydroxycholesterol restrains the transcriptional regulator SREBP2 and limits intestinal IgA plasma cell differentiation. Immunity 54, 2273–2287.e6. 10.1016/j.immuni.2021.09.004. [PubMed: 34644558]
30. Tas JMJ, Mesin L, Pasqual G, Targ S, Jacobsen JT, Mano YM, Chen CS, Weill JC, Reynaud CA, Browne EP, et al. (2016). Visualizing antibody affinity maturation in germinal centers. Science 351, 1048–1054. 10.1126/science.aad3439. [PubMed: 26912368]
31. Phan TG, Paus D, Chan TD, Turner ML, Nutt SL, Basten A, and Brink R (2006). High affinity germinal center B cells are actively selected into the plasma cell compartment. Journal of Experimental Medicine 203, 2419–2424. 10.1084/jem.20061254. [PubMed: 17030950]
32. Victora GD, and Nussenzweig MC (2022). Germinal Centers. Annu Rev Immunol 40, 1–30. 10.1146/annurev-immunol-120419-022408. [PubMed: 34871102]
33. Biram A, Winter E, Denton AE, Zaretsky I, Dassa B, Bemark M, Linterman MA, Yaari G, and Shulman Z (2020). B Cell Diversification Is Uncoupled from SAP-Mediated Selection Forces in Chronic Germinal Centers within Peyer's Patches. Cell Reports 30, 1910–1922.e5. 10.1016/j.celrep.2020.01.032. [PubMed: 32049020]
34. Razzaghi R, Agarwal S, Kotlov N, Plotnikova O, Nomie K, Huang DW, Wright GW, Smith GA, Li M, Takata K, et al. (2021). Compromised counterselection by FAS creates an aggressive subtype of germinal center lymphoma. J Exp Med 218, 248. 10.1084/jem.20201173.
35. Chen H, Zhang Y, Ye AY, Du Z, Xu M, Lee C-S, Hwang JK, Kyritsis N, Ba Z, Neuberg D, et al. (2020). BCR selection and affinity maturation in Peyer's patch germinal centres. Nature 582, 1–23. 10.1038/s41586-020-2262-4.
36. Nowosad CR, Mesin L, Castro TBR, Wichmann C, Donaldson GP, Araki T, Schiepers A, Lockhart AAK, Bilate AM, Mucida D, et al. (2020). Tunable dynamics of B cell selection in gut germinal centres. Nature 6, 122–126. 10.1038/s41586-020-2865-9.
37. Luo W, Weisel F, and Shlomchik MJ (2018). B Cell Receptor and CD40 Signaling Are Rewired for Synergistic Induction of the c-Myc Transcription Factor in Germinal Center B Cells. Immunity 48, 313–326.e5. 10.1016/j.immuni.2018.01.008. [PubMed: 29396161]
38. Davidzohn N, Biram A, Stoler-Barak L, Grenov A, Dassa B, and Shulman Z (2019). Syk degradation restrains plasma cell formation and promotes zonal transitions in germinal centers. Journal of Experimental Medicine 217, 26648–26. 10.1084/jem.20191043.
39. Victora GD, Schwickert TA, Fooksman DR, Kamphorst AO, Meyer-Hermann M, Dustin ML, and Nussenzweig MC (2010). Germinal Center Dynamics Revealed by Multiphoton Microscopy with a Photoactivatable Fluorescent Reporter. Cell 143, 592–605. 10.1016/j.cell.2010.10.032. [PubMed: 21074050]
40. Ersching J, Efeyan A, Mesin L, Jacobsen JT, Pasqual G, Grabiner BC, Dominguez-Sola D, Sabatini DM, and Victora GD (2017). Germinal Center Selection and Affinity Maturation Require Dynamic Regulation of mTORC1 Kinase. Immunity 46, 1045–1058.e6. 10.1016/j.immuni.2017.06.005. [PubMed: 28636954]
41. Gitlin AD, Shulman Z, and Nussenzweig MC (2014). Clonal selection in the germinal centre by regulated proliferation and hypermutation. Nature 509, 1–9. 10.1038/nature13300.
42. Yang Z, Robinson MJ, Chen X, Smith GA, Taunton J, Liu W, and Allen CDC (2016). Regulation of B cell fate by chronic activity of the IgE B cell receptor. eLife 5, 409. 10.7554/elife.21238.

43. Sundling C, Lau AWY, Bourne K, Young C, Laurianto C, Hermes JR, Menzies RJ, Butt D, Kräutler NJ, Zahra D, et al. (2021). Positive selection of IgG+ over IgM+ B cells in the germinal center reaction. Immunity 54, 988–1001.e5. 10.1016/j.immuni.2021.03.013. [PubMed: 33857421]
44. Newman R, and Tolar P (2021). Chronic calcium signaling in IgE+ B cells limits plasma cell differentiation and survival. Immunity. 10.1016/j.immuni.2021.11.006.
45. Haniuda K, Fukao S, Kodama T, Hasegawa H, and Kitamura D (2016). Autonomous membrane IgE signaling prevents IgE-memory formation. Nat Immunol 17, 1109–1117. 10.1038/ni.3508. [PubMed: 27428827]
46. Harriman GR, Bradley A, Das S, Rogers-Fani P, and Davis AC (1996). IgA class switch in I alpha exon-deficient mice. Role of germline transcription in class switch recombination. J Clin Invest 97, 477–485. 10.1172/jci118438. [PubMed: 8567970]
47. Bannard O, and Cyster JG (2017). ScienceDirect Germinal centers: programmed for affinity maturation and antibody diversification. Current Opinion in Immunology 45, 21–30. 10.1016/j.coi.2016.12.004. [PubMed: 28088708]
48. Taylor JJ, Pape KA, and Jenkins MK (2012). A germinal center–independent pathway generates unswitched memory B cells early in the primary response. J Exp Medicine 209, 597–606. 10.1084/jem.20111696.
49. Martinoli C, Chiavelli A, and Rescigno M (2007). Entry Route of Salmonella typhimurium Directs the Type of Induced Immune Response. Immunity 27, 975–984. 10.1016/j.immuni.2007.10.011. [PubMed: 18083577]
50. Biram A, Liu J, Hezroni EL, Davidzohn N, Schmiedel D, Khatib-Massalha E, Haddad M, Grenov A, Lebon S, Salame TM, et al. (2022). Bacterial infection disrupts established germinal center reactions through monocyte recruitment and impaired metabolic adaptation. Immunity. 10.1016/j.immuni.2022.01.013.
51. Gohda M, Kunisawa J, Miura F, Kagiyama Y, Kurashima Y, Higuchi M, Ishikawa I, Ogahara I, and Kiyono H (2008). Sphingosine 1-phosphate regulates the egress of IgA plasmablasts from Peyer's patches for intestinal IgA responses. J Immunol 180, 5335–5343. 10.4049/jimmunol.180.8.5335. [PubMed: 18390715]
52. Wagner N, Löhler J, Kunkel EJ, Ley K, Leung E, Krissansen G, Rajewsky K, and Müller W (1996). Critical role for beta7 integrins in formation of the gut-associated lymphoid tissue. Nature 382, 366–370. 10.1038/382366a0. [PubMed: 8684468]
53. Farstad IN, Halstensen TS, Lazarovits AI, Norstein J, Fausa O, and Brandtzaeg P (1995). Human intestinal B-cell blasts and plasma cells express the mucosal homing receptor integrin alpha 4 beta 7. Scand J Immunol 42, 662–672. 10.1111/j.1365-3083.1995.tb03709.x. [PubMed: 8552990]
54. Pabst O, Ohl L, Wendland M, Wurbel M-A, Kremmer E, Malissen B, and Förster R (2004). Chemokine receptor CCR9 contributes to the localization of plasma cells to the small intestine. Journal of Experimental Medicine 199, 411–416. 10.1084/jem.20030996. [PubMed: 14744993]
55. Crawford PA, and Gordon JI (2005). Microbial regulation of intestinal radiosensitivity. Proc National Acad Sci 102, 13254–13259. 10.1073/pnas.0504830102.
56. Koch MA, Reiner GL, Lugo KA, Kreuk LSM, Stanbery AG, Ansaldo E, Seher TD, Ludington WB, and Barton GM (2016). Maternal IgG and IgA Antibodies Dampen Mucosal T Helper Cell Responses in Early Life. Cell 165, 827–841. 10.1016/j.cell.2016.04.055. [PubMed: 27153495]
57. Lycke N, and Bemark M (2010). Mucosal adjuvants and long-term memory development with special focus on CTA1-DD and other ADP-ribosylating toxins. Mucosal Immunol 3, 1–11. 10.1038/mi.2010.54.
58. Mayer CT, Gazumyan A, Kara EE, Gitlin AD, Golijanin J, Viant C, Pai J, Oliveira TY, Wang Q, Escolano A, et al. (2017). The microanatomic segregation of selection by apoptosis in the germinal center. Science 358, eaao2602–14. 10.1126/science.aao2602. [PubMed: 28935768]
59. Stewart I, Radtke D, Phillips B, McGowan SJ, and Bannard O (2018). Germinal Center B Cells Replace Their Antigen Receptors in Dark Zones and Fail Light Zone Entry when Immunoglobulin Gene Mutations are Damaging. Immunity 49, 477–489.e7. 10.1016/j.immuni.2018.08.025. [PubMed: 30231983]

60. Long Z, Phillips B, Radtke D, Meyer-Hermann M, and Bannard O (2022). Competition for refueling rather than cyclic reentry initiation evident in germinal centers. Sci Immunol 7, eabm0775. 10.1126/sciimmunol.abm0775. [PubMed: 35275753]

61. Dominguez-Sola D, Victora GD, Ying CY, Phan RT, Saito M, Nussenzweig MC, and Dalla-Favera R (2012). The proto-oncogene MYC is required for selection in the germinal center and cyclic reentry. Nat Immunol 13, 1083–1091. 10.1038/ni.2428. [PubMed: 23001145]

62. Calado DP, Sasaki Y, Godinho SA, Pellerin A, Köchert K, Sleckman BP, Alborán I.M. de, Janz M, Rodig S, and Rajewsky K (2012). MYC is essential for the formation and maintenance of germinal centers. Nat Immunol 13, 1092–1100. 10.1038/ni.2418. [PubMed: 23001146]

63. Khalil AM, Cambier JC, and Shlomchik MJ (2012). B Cell Receptor Signal Transduction in the GC Is Short-Circuited by High Phosphatase Activity. Science 336, 1178–1181. 10.1126/science.1213368. [PubMed: 22555432]

64. Stavnezer J, Sirlin S, and Abbott J (1985). Induction of immunoglobulin isotype switching in cultured I.29 B lymphoma cells. Characterization of the accompanying rearrangements of heavy chain genes. Journal of Experimental Medicine 161, 577–601. 10.1084/jem.l61.3.577. [PubMed: 2579186]

65. Nakamura M, Kondo S, Sugai M, Nazarea M, Imamura S, and Honjo T (1996). High frequency class switching of an lgM+ B lymphoma clone CH12F3 to lgA+ cells. Int Immunol 8, 193–201. 10.1093/intimm/8.2.193. [PubMed: 8671604]

66. Catlett IM, and Bishop GA (1999). Cutting edge: a novel mechanism for rescue of B cells from CD95/Fas-mediated apoptosis. J Immunol 163, 2378–2381. [PubMed: 10452970]

67. Rothstein TL, Wang JKM, Panka DJ, Foote LC, Wang Z, Stanger B, Cui H, Ju S-T, and Marshak-Rothstein A (1995). Protection against Fas-dependent Thl-mediated apoptosis by antigen receptor engagement in B cells. Nature 374, 163–165. 10.1038/374163a0. [PubMed: 7533263]

68. Xiao S, Jodo S, Sung SJ, Marshak-Rothstein A, and Ju S-T (2002). A Novel Signaling Mechanism for Soluble CD95 Ligand SYNERGY WITH ANTI-CD95 MONOCLONAL ANTIBODIES FOR APOPTOSIS AND NF-κB NUCLEAR TRANSLOCATION*. J Biol Chem 277, 50907–50913. 10.1074/jbc.m206093200. [PubMed: 12393889]

69. Hohlbaum AM, Gregory MS, Ju ST, and Marshak-Rothstein A (2001). Fas ligand engagement of resident peritoneal macrophages in vivo induces apoptosis and the production of neutrophil chemotactic factors. J Immunol 167, 6217–6224. 10.4049/jimmunol.167.11.6217. [PubMed: 11714783]

70. Takahashi Y, Ohta H, and Takemori T (2001). Fas Is Required for Clonal Selection in Germinal Centers and the Subsequent Establishment of the Memory B Cell Repertoire. Immunity 14, 181–192. 10.1016/s1074-7613(01)00100-5. [PubMed: 11239450]

71. Smith KG, Nossal GJ, and Tarlinton DM (1995). FAS is highly expressed in the germinal center but is not required for regulation of the B-cell response to antigen. Proc National Acad Sci 92, 11628–11632. 10.1073/pnas.92.25.11628.

72. Butt D, Chan TD, Bourne K, Hermes JR, Nguyen A, Statham A, O'Reilly LA, Strasser A, Price S, Schofield P, et al. (2015). FAS Inactivation Releases Unconventional Germinal Center B Cells that Escape Antigen Control and Drive IgE and Autoantibody Production. Immunity 42, 890–902. 10.1016/j.immuni.2015.04.010. [PubMed: 25979420]

73. Johansen F-E, Braathen R, and Brandtzaeg P (2000). Role of J chain in secretory immunoglobulin formation. Scandinavian Journal of Immunology 52, 240–248. 10.1046/j.1365-3083.2000.00790.x. [PubMed: 10972899]

74. Lycke N, Erlandsson L, Ekman L, Schön K, and Leanderson T (1999). Lack of J chain inhibits the transport of gut IgA and abrogates the development of intestinal antitoxic protection. J Immunol Baltim Md 1950 163, 913–919.

75. Woof JM, and Russell MW (2019). Structure and function relationships in IgA. Mucosal Immunol 4, 1–8. 10.1038/mi.2011.39.

76. Chen ST, Oliveira TY, Gazumyan A, Cipolla M, and Nussenzweig MC (2023). B cell receptor signaling in germinal centers prolongs survival and primes B cells for selection. Immunity 56, 547–561.e7. 10.1016/j.immuni.2023.02.003. [PubMed: 36882061]

77. Nowosad CR, Spillane KM, and Tolar P (2016). Germinal center B cells recognize antigen through a specialized immune synapse architecture. Nat Immunol 17, 870–877. 10.1038/ni.3458. [PubMed: 27183103]

78. Wan Z, Zhang S, Fan Y, Liu K, Du F, Davey AM, Zhang H, Han W, Xiong C, and Liu W (2013). B Cell Activation Is Regulated by the Stiffness Properties of the Substrate Presenting the Antigens. J Immunol 190, 4661–4675. 10.4049/jimmunol.1202976. [PubMed: 23554309]

79. Paus D, Phan TG, Chan TD, Gardam S, Basten A, and Brink R (2006). Antigen recognition strength regulates the choice between extrafollicular plasma cell and germinal center B cell differentiation. Journal of Experimental Medicine 203, 1081–1091. 10.1084/jem.20060087. [PubMed: 16606676]

80. Muppidi JR, Schmitz R, Green JA, Xiao W, Larsen AB, Braun SE, An J, Xu Y, Rosenwald A, Ott G, et al. (2014). Loss of signalling via Gα13 in germinal centre B-cell-derived lymphoma. Nature 516, 254–258. 10.1038/nature13765. [PubMed: 25274307]

81. Green JA, Suzuki K, Cho B, Willison LD, Palmer D, Allen CDC, Schmidt TH, Xu Y, Proia RL, Coughlin SR, et al. (2011). The sphingosine 1-phosphate receptor S1P2 maintains the homeostasis of germinal center B cells and promotes niche confinement. Nat Immunol 12, 672–680. 10.1038/ni.2047. [PubMed: 21642988]

82. Wittner J, Schulz SR, Steinmetz TD, Berges J, Hauke M, Channell WM, Cunningham AF, Hauser AE, Hutloff A, Mielenz D, et al. (2022). Krüppel-like factor 2 controls IgA plasma cell compartmentalization and IgA responses. Mucosal Immunol, 1–15. 10.1038/s41385-022-00503-0. [PubMed: 34239028]

83. Pinto D, Montani E, Bolli M, Garavaglia G, Sallusto F, Lanzavecchia A, and Jarrossay D (2013). A functional BCR in human IgA and IgM plasma cells. Blood 121, 4110–4114. 10.1182/blood-2012-09-459289. [PubMed: 23550036]

84. Price MJ, Hicks SL, Bradley JE, Randall TD, Boss JM, and Scharer CD (2019). IgM, IgG, and IgA Influenza-Specific Plasma Cells Express Divergent Transcriptomes. J Immunol 203, 2121–2129. 10.4049/jimmunol.1900285. [PubMed: 31501259]

85. Martin JC, Chang C, Boschetti G, Ungaro R, Giri M, Grout JA, Gettler K, Chuang L, Nayar S, Greenstein AJ, et al. (2019). Single-Cell Analysis of Crohn's Disease Lesions Identifies a Pathogenic Cellular Module Associated with Resistance to Anti-TNF Therapy. Cell 178, 1493–1508.e20. 10.1016/j.cell.2019.08.008. [PubMed: 31474370]

86. Zeng MY, Cisalpino D, Varadarajan S, Hellman J, Warren HS, Cascalho M, Inohara N, and Núñez G (2016). Gut Microbiota-Induced Immunoglobulin G Controls Systemic Infection by Symbiotic Bacteria and Pathogens. Immunity 44, 1–23. 10.1016/j.immuni.2016.02.006. [PubMed: 26789912]

87. Scheid JF, Eraslan B, Hudak A, Brown EM, Sergio D, Delorey TM, Phillips D, Lefkovith A, Jess AT, Duck LW, et al. (2023). Remodeling of colon plasma cell repertoire within ulcerative colitis patients. J Exp Med 220, e20220538. 10.1084/jem.20220538. [PubMed: 36752797]

88. Ceglia S, Berthelette A, Howley K, Li Y, Mortzfeld B, Bhattarai SK, Yiew NKH, Xu Y, Brink R, Cyster JG, et al. (2023). An epithelial cell-derived metabolite tunes immunoglobulin A secretion by gut-resident plasma cells. Nat Immunol, 1–14. 10.1038/s41590-022-01413-w.

89. Kuraoka M, Schmidt AG, Nojima T, Feng F, Watanabe A, Kitamura D, Harrison SC, Kepler TB, and Kelsoe G (2016). Complex Antigens Drive Permissive Clonal Selection in Germinal Centers. Immunity, 1–30. 10.1016/j.immuni.2016.02.010.

90. Jodo S, Xiao S, Hohlbaum A, Strehlow D, Marshak-Rothstein A, and Ju S-T (2001). Apoptosis-inducing Membrane Vesicles A NOVEL AGENT WITH UNIQUE PROPERTIES*. J Biol Chem 276, 39938–39944. 10.1074/jbc.m107005200. [PubMed: 11546786]

Highlights

- IgA BCR underpins PP GC competitiveness, memory B cell and plasma cell generation
- IgA BCR drives stronger intracellular signaling in GC B cells in vitro and ex vivo
- IgA+ GC B cells receive increased T cell help and resist FasL-induced cell death
- IgA BCR, not Fas-FasL axis, controls differentiation into gut-homing plasma cells

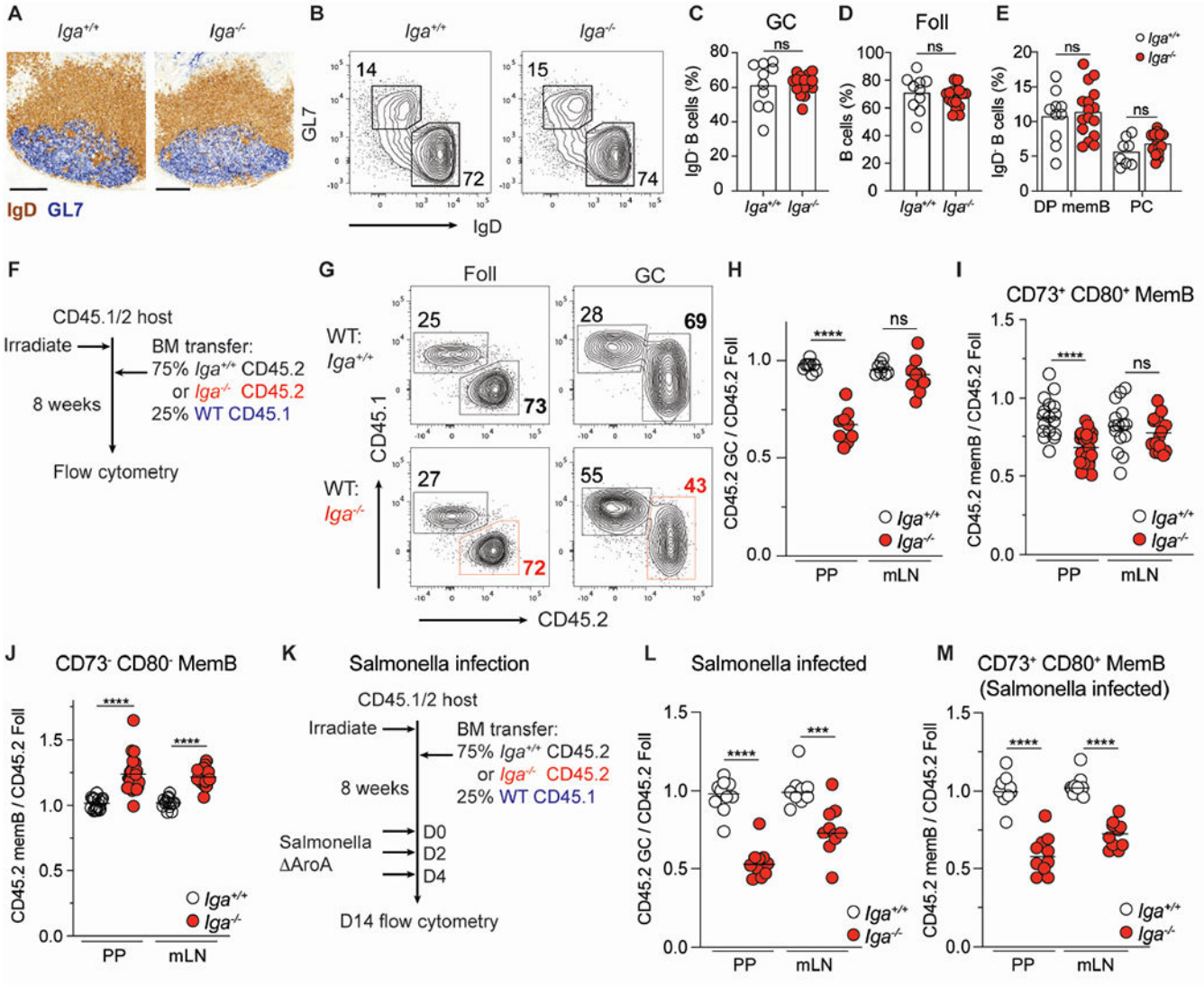

Figure 1. IgA^{+} B cells dominate the germinal center reaction and are preferentially selected into the memory compartment.

(A-E) Steady state, co-housed, 8–12-week-old *Iga*$^{+/+}$ and *Iga*$^{-/-}$ mice.

(A) Frozen PP sections from *Iga*$^{+/+}$ and *Iga*$^{-/-}$ mice stained with immunohistochemistry antibodies against IgD (brown) and GL7 (blue). Scale bars, 200 μm.

(B) Representative plot of PP GC (GL7^{+} IgD^{-}) and Foll (GL7^{-} IgD^{+}) B cells in *Iga*$^{+/+}$ and *Iga*$^{-/-}$ mice. Gated on live CD138^{-} B cells.

(C) PP GC B cells as percentage of activated (IgD^{-}) B cells.

(D) PP Foll B cells as percentage of B cells.

(E) CD73^{+} CD80^{+} (DP) MemB, PCs as percentage of activated B cells.

(F) *Iga*$^{-/-}$ mixed BM chimera experimental set up for (G-J).

(G) Representative CD45 staining on Foll and GC B cells in mixed BM chimeras.

(H) Ratio of frequency of CD45.2 GC B cells to CD45.2 Foll B cells in PP and mLN.

(I, J) Ratio of frequency of CD45.2 DP memB cells (I) or CD45.2 CD73^{-} CD80^{-} (DN) MemB cells (J) to CD45.2 Foll B cells in PP and mLN.

(K) Salmonella infection experimental setup in *Iga*$^{-/-}$ mixed BM chimera for (L-M).
(L) Ratio of frequency of CD45.2 GC B cells to CD45.2 Foll B cells in PP and mLN of Salmonella infected chimeras.
(M) Ratio of frequency of CD45.2 DP MemB cells to CD45.2 Foll B cells in PP and mLN of Salmonella infected chimeras.
Data from at least 3 independent experiments with 2-3 mice per group (A-M). Each symbol represents one mouse. ns=not significant; ***p < 0.0005; ****p < 0.0001; Unpaired two-tailed Student's t-test.
See also Figure S1.

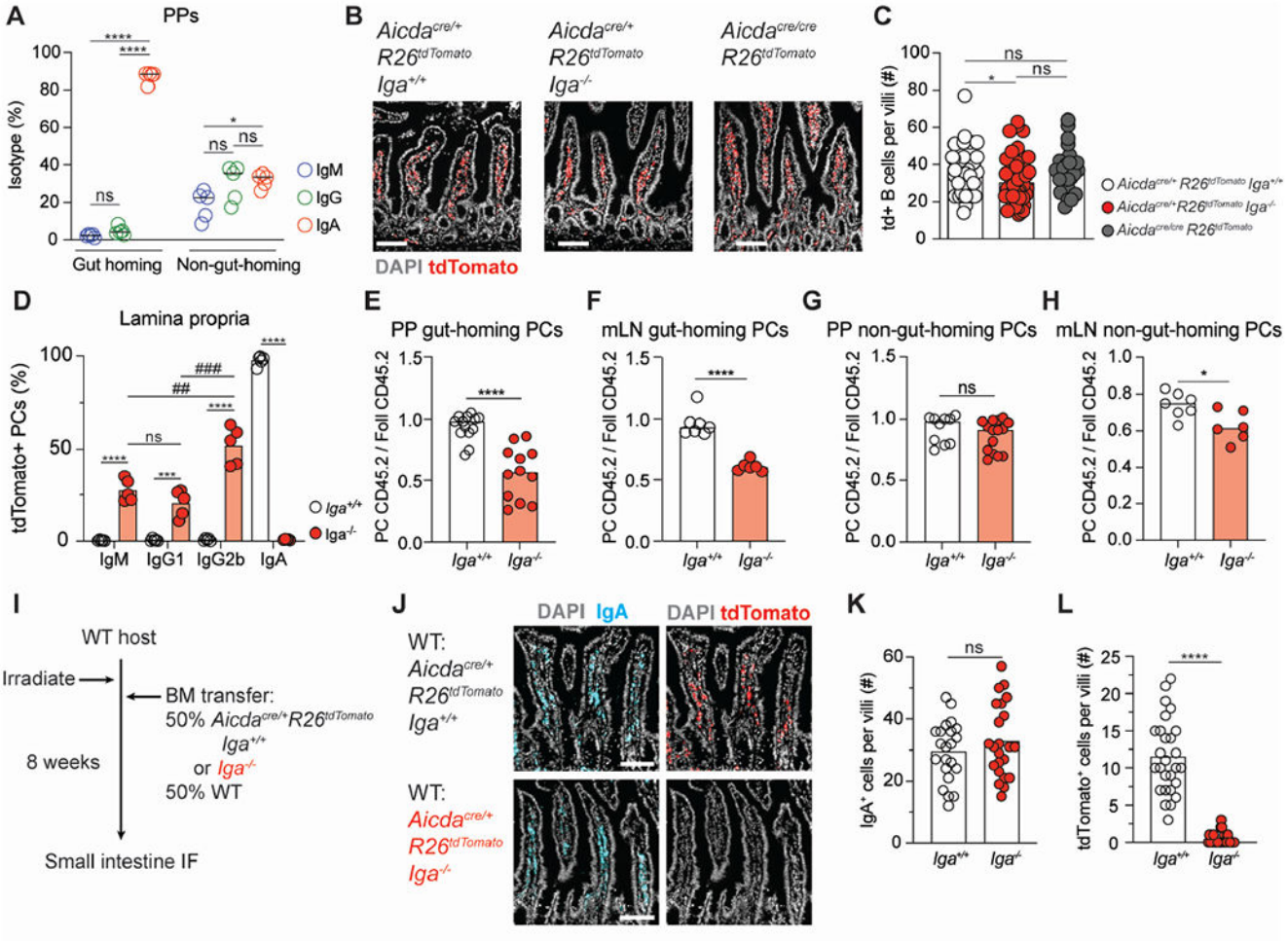

Figure 2. IgA is required for efficient plasma cell homing to the intestinal lamina propria.

(A) Isotypes of gut-homing ($\alpha4\beta7^+$ $CCR9^+$) and non-gut homing PCs from PPs of WT mice treated with FTY-720 for seven days. IgG is defined as $IgG1^+$ or $IgG2b^+$.

(B) Representative immunofluorescence of small intestinal villi from *Aicda*$^{cre/+}$ *Rosa26*$^{Stop\text{-}tdTomato}$ *Iga*$^{+/+}$, *Aicda*$^{cre/+}$ *Rosa26*$^{Stop\text{-}tdTomato}$ *Iga*$^{-/-}$, *Aicda*$^{cre/cre}$ *Rosa26*$^{Stop\text{-}tdTomato}$ mice stained with DAPI (gray) and tdTomato (red). Scale bars, 100 μm.

(C) Quantification of multiple images as in (B). Number of $tdTom^+$ cells per villi.

(D) Isotype staining in *Aicda*$^{cre/+}$ *Rosa26*$^{Stop\text{-}tdTomato}$ *Iga*$^{+/+}$ and *Aicda*$^{cre/+}$ *Rosa26*$^{Stop\text{-}tdTomato}$ *Iga*$^{-/-}$ lamina propria. Gated on $CD98^+$ $B220^-$ $CD4^-$ PCs.

(E, F) Ratio of frequency of CD45.2 gut-homing PCs to CD45.2 Foll B cells from PPs (E) or mLN (F) of mixed BM chimeras.

(G, H) Ratio of frequency of CD45.2 non-gut-homing PCs to CD45.2 Foll B cells from PPs (G) or mLN (H) of mixed BM chimeras.

(I) *Aicda*$^{cre/+}$ *Rosa26*$^{Stop\text{-}tdTomato}$ *Iga*$^{+/+}$ mixed BM chimera experimental set up for (J-L).

(J) Representative immunofluorescence of small intestinal villi stained for DAPI (gray), IgA (cyan), and tdTomato (red) in WT: *Aicda*^{cre} *Rosa26*$^{Stop\text{-}tdTomato}$ *Iga*$^{+/+}$ or *Iga*$^{-/-}$ mixed BM chimeras. Scale bars, 100 μm.

(K, L) Quantification of multiple images as in (J). Number of IgA^+ cells (K) or $tdTom^+$ cells (L) per villi.

Data from 2 independent experiments with 2-3 mice per group (A, C, D, K, L). Data from at least 3 independent experiments with 3-5 mice per group (E-H). Each symbol represents one mouse. (C, K, L) Each symbol represents one villi with at least 5 villi quantified per image. ns=not significant, *p < 0.005; ##p < 0.001; ***, ###p < 0.0005; ****p < 0.0001. Unpaired two-tailed Student's t-test in E-H, K, L. One way ANOVA was used in A(*), C(*), and D(#) .

See also Figure S2.

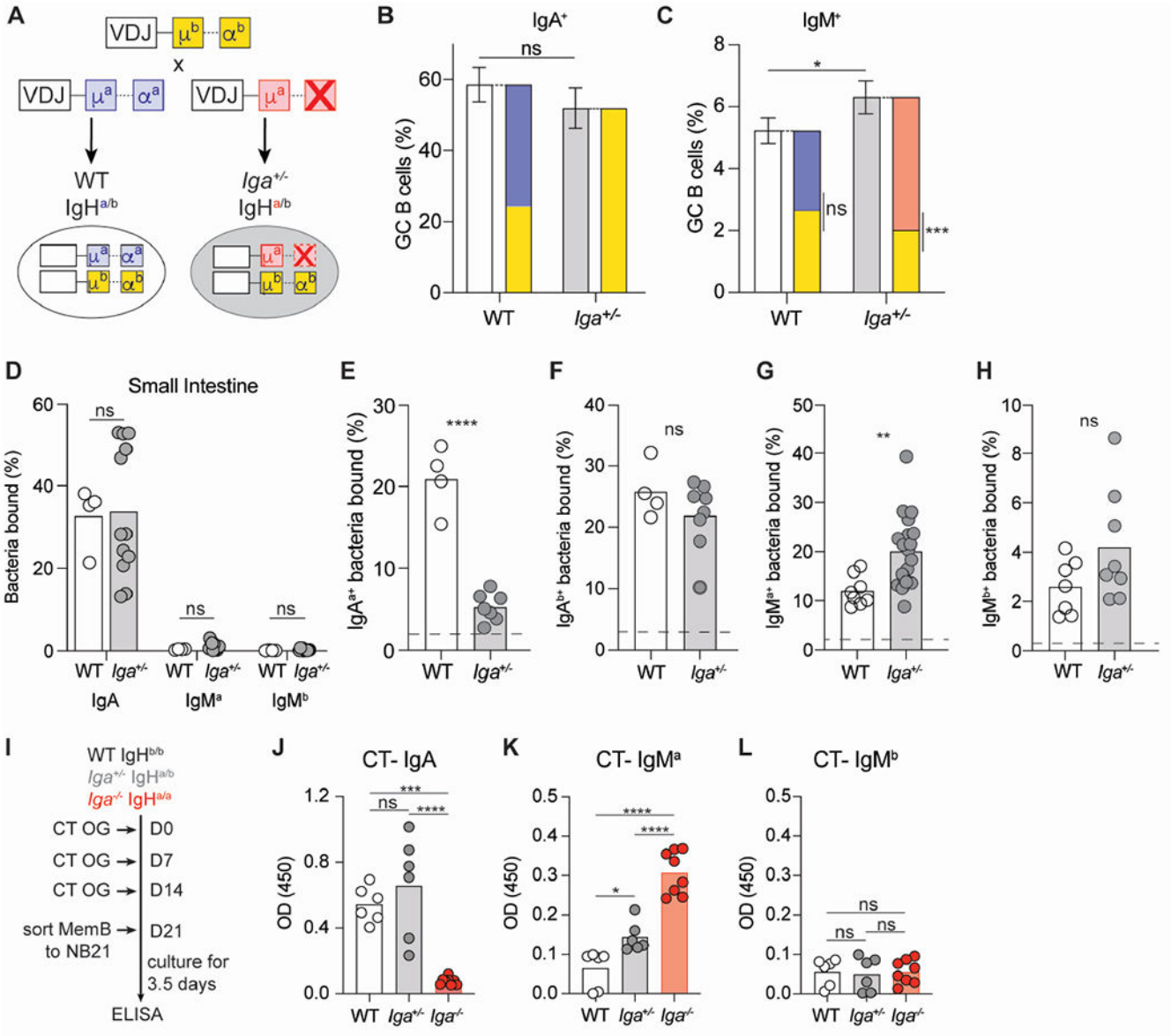

Figure 3. IgA is dominant in activated B cells of intrinsic chimera mice.

(A) Breeding setup for WT IgH$^{a/b}$ and *Iga*$^{+/-}$ IgH$^{a/b}$ mice.

(B, C) Percentage of IgA^{+} (B) and IgM^{+} (C) GC B cells in PPs. Solid bars represent indicated total isotype in GC; stacked bars represent allotypic isotype in GC of WT and *Iga*$^{+/-}$ mice.

(D) Percentage of endogenously coated small intestinal bacteria with indicated antibodies.

(E, F) Percentage of intestinal commensal from μMT mice stained by IgA^{a} (E) or IgA^{b} (F) antibodies from *Iga*$^{+/+}$ or *Iga*$^{+/-}$ serum.

(G, H) Percentage of intestinal commensal bacteria from μMT mice stained by IgM^{a} (G) or IgM^{b} (H) antibodies from *Iga*$^{+/+}$ or *Iga*$^{+/-}$ serum. Dashed line represents unstained μMT bacteria in E-H.

(I) Experimental setup for cholera toxin(CT) oral immunization and subsequent MemB cell in vitro culture with NB21 feeder cells.
(J, K, L) ELISA OD for CT specific IgA (J), IgM^a (K), and IgM^b (L) antibodies detected in MemB supernatant 3.5 days after in vitro culture.
Data from at least 3 independent experiments with 2-3 mice per group (B-H). Data from 4 independent experiments with 1-3 mice per group (J-L). ns=not significant, *$p < 0.005$; **$p < 0.001$; ***$p < 0.0005$; ****$p < 0.0001$; Unpaired two-tailed Student's t-test in B-H. One way ANOVA in J-L.
See also Figure S2.

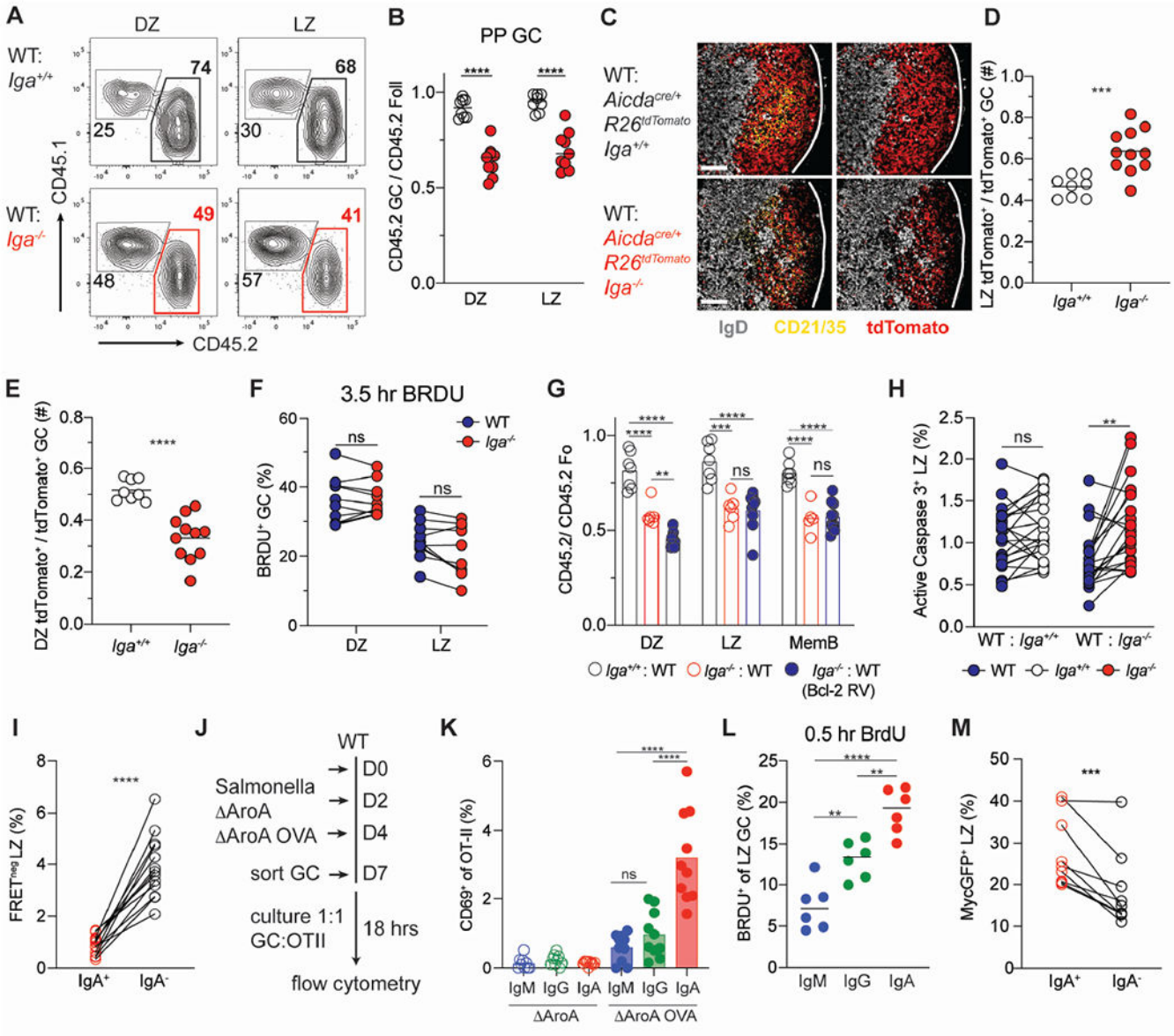

Figure 4. IgA^{+} B cells exhibit higher cell death resistance and experience stronger T cell-dependent help in GC LZ.

(A) Representative CD45 staining on PP GC LZ (CXCR4^{lo} CD86^{hi}) and DZ (CXCR4^{hi} CD86^{hi}) B cells in mixed BM chimeras.

(B) Ratio of frequency of CD45.2 DZ or LZ B cells to CD45.2 Foll B cells in PP of mixed BM chimeras.

(C) Representative PP immunofluorescence stained for DAPI (gray), tdTomato (red) and CD21/35 (cyan), in WT: *Aicda*$^{cre/+}$ *Rosa26*$^{Stop\text{-}tdTomato}$ *Iga*$^{+/+}$ or *Iga*$^{-/-}$ mixed BM chimeras. Scale bars, 100 μm. Lines indicate GC edges with LZ oriented on left, DZ right.

(D, E) Guantification of multiple images as in (C). Ratio of frequency of tdTom^{+} cells in LZ (D) or DZ (E) to total TdTom^{+} GC B cells.

(F) Percentage of BrdU^{+} DZ or LZ GC B cells in PPs of *Iga*$^{-/-}$:WT mixed BM chimeras after 3.5 hour BrdU pulse.

(G) Ratio of frequency of indicated CD45.2 B cells to CD45.2 Foll B cells in PP of WT *Bcl2*: *Iga*$^{-/-}$ *Bcl2* retroviral mixed BM chimeras.
(H) Percentage of active caspase3^{+} LZ GC B cells in mixed BM chimeras.
(I) Percentage of FRET negative LZ IgA^{+} and IgA^{-} cells from *Rosa26*^{INDIA} PPs.
(J) Experimental set up for Salmonella ΔAroA infection and in vitro GC antigen presentation in (K).
(K) Percentage of CD69^{+} CD4^{+} OT-II T cells co-cultured with indicated GC B cell isotype. PP GC subsets were sorted according to isotype expression (IgG = IgG1^{+} or IgG2b^{+}). Mice were infected with Salmonella ΔAroA expressing or not expressing OVA (ΔAroA or ΔAroAOVA). Each symbol is the average of technical replicates from one mouse.
(L) Percentage of BrdU^{+} LZ GC B cells in PPs for indicated isotypes after 30-minute BrdU pulse. GC subsets were gated according to isotype expression (IgG = IgM^{-} IgA^{-}).
(M) Percentage of cMycGFP^{+} LZ IgA^{+} and IgA^{-} B cells from cMyc-GFP PPs
Data are from at least 3 independent experiments with at least 3 mice per group (B, F, H, I, M, K). Data are from 2 experiments with 2-3 mice per group (C-E, G, L). ns=not significant, **p < 0.001; ***p < 0.0005; ****p < 0.0001. Unpaired two-tailed Student's t-test in B, D, E, F, H, I, M. One-way ANOVA in G, K, L.
See also Figure S3.

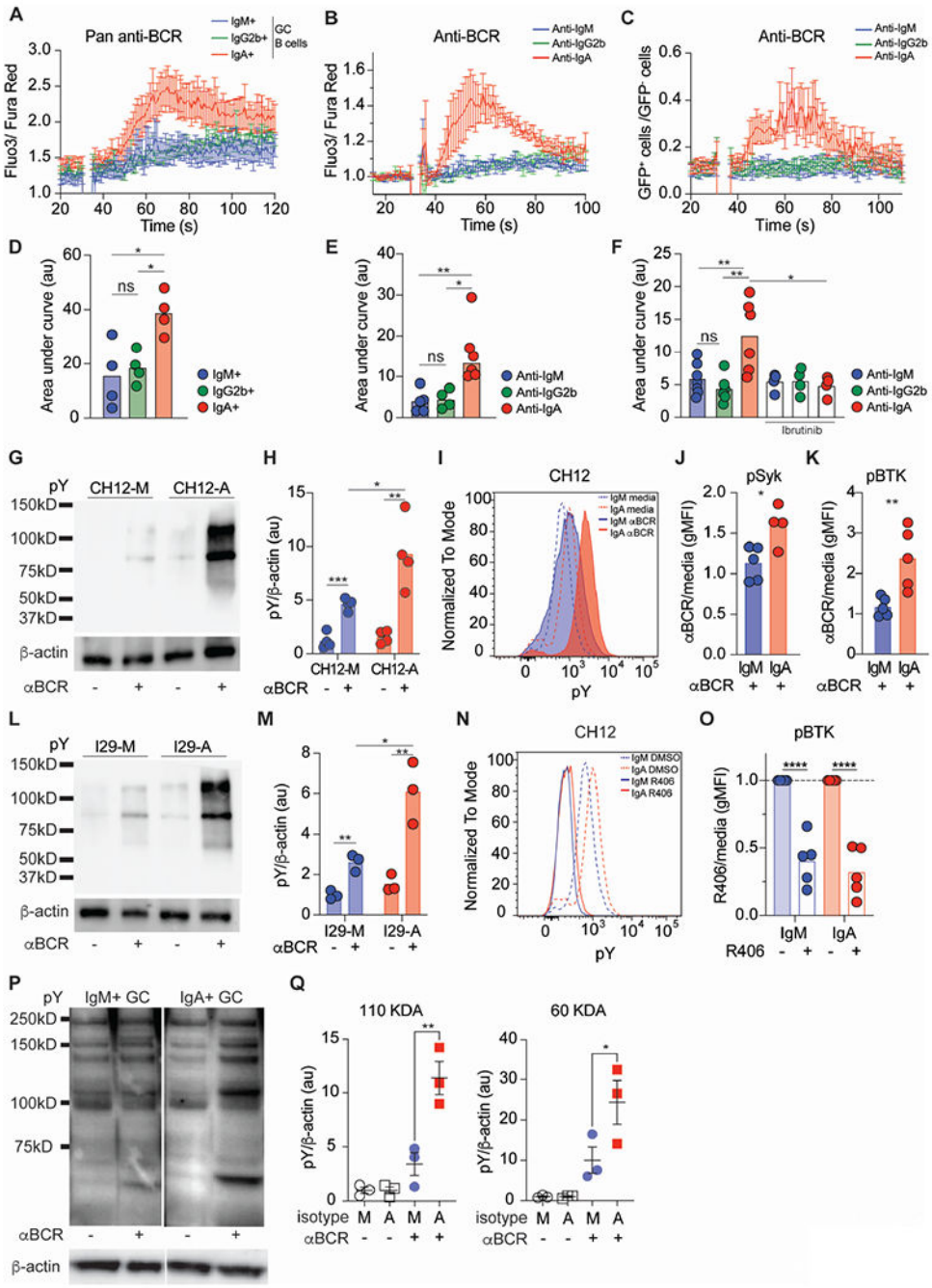

Figure 5. Enhanced BCR signaling in murine and human IgA$^+$ GC B cells.

(A) Compiled calcium traces for IgM, IgG2b, and IgA PP GC B cells (defined as isotype negative populations) stimulated with pan anti-BCR.

(B) Compiled calcium traces for *Aicda*$^{cre/+}$ *Rosa26*$^{Stop\text{-}tdTomato/+}$ PP GC B cells stimulated with indicated anti-BCR isotypes.

(C) Compiled calcium traces from *Aicda*$^{cre/+}$ *Rosa26*$^{Stop\text{-}tdTomato/gCAMP}$ PP GC B cells stimulated with indicated anti-BCR isotypes. Shown as ratio of frequency of gCAMP-GFP$^+$ to gCAMP-GFP$^-$ cells per second.

(D) Area under the curve(AUC) of individual calcium traces calculated between 50 and 100 seconds for (A).
(E) AUC of individual calcium traces calculated between 40 and 100 seconds for (B).
(F) AUC of individual calcium traces calculated between 40 and 100 seconds for (C) Indicated samples were pre-treated with ibrutinib prior to anti-BCR stimulation.
(G) Representative pY and β-actin western blots for CH12 cells stimulated with anti-BCR.
(H) Quantitative analysis from (G) of pY normalized to β-actin.
(I) Representative histogram of pY in CH12 cells after BCR stimulation.
(J, K) pSyk (J) or pBTK (K) gMFI normalized to untreated(media) in CH12 cells after anti-BCR.
(L) Representative pY and β-actin western blot for I29 cells stimulated with anti-BCR.
(M) Quantitative analysis from (L) of pY normalized to β-actin.
(N) Representative pY histogram in CH12 cells after R406 incubation.
(O) pBTK gMFI normalized to untreated(media) after R406 incubation in CH12 cells.
(P) Representative pY and β-actin western blots from GC human tonsils of indicated isotypes after anti-BCR stimulation. Sorted as isotype negative populations.
(Q) Quantitative analysis from (P) of pY normalized to β-actin.
A, D, H are compiled data from 4 independent experiments. B, C, E, F, J, K, O, Q are compiled data from at least 3 independent experiments. ns=not significant, *p < 0.005; **p < 0.001; ***p < 0.0005; ****p < 0.0001. Unpaired two-tailed Student’s t-test in J, K, O. One-way ANOVA in D, E, F, H, M, Q.
See also Figure S4 and S5.

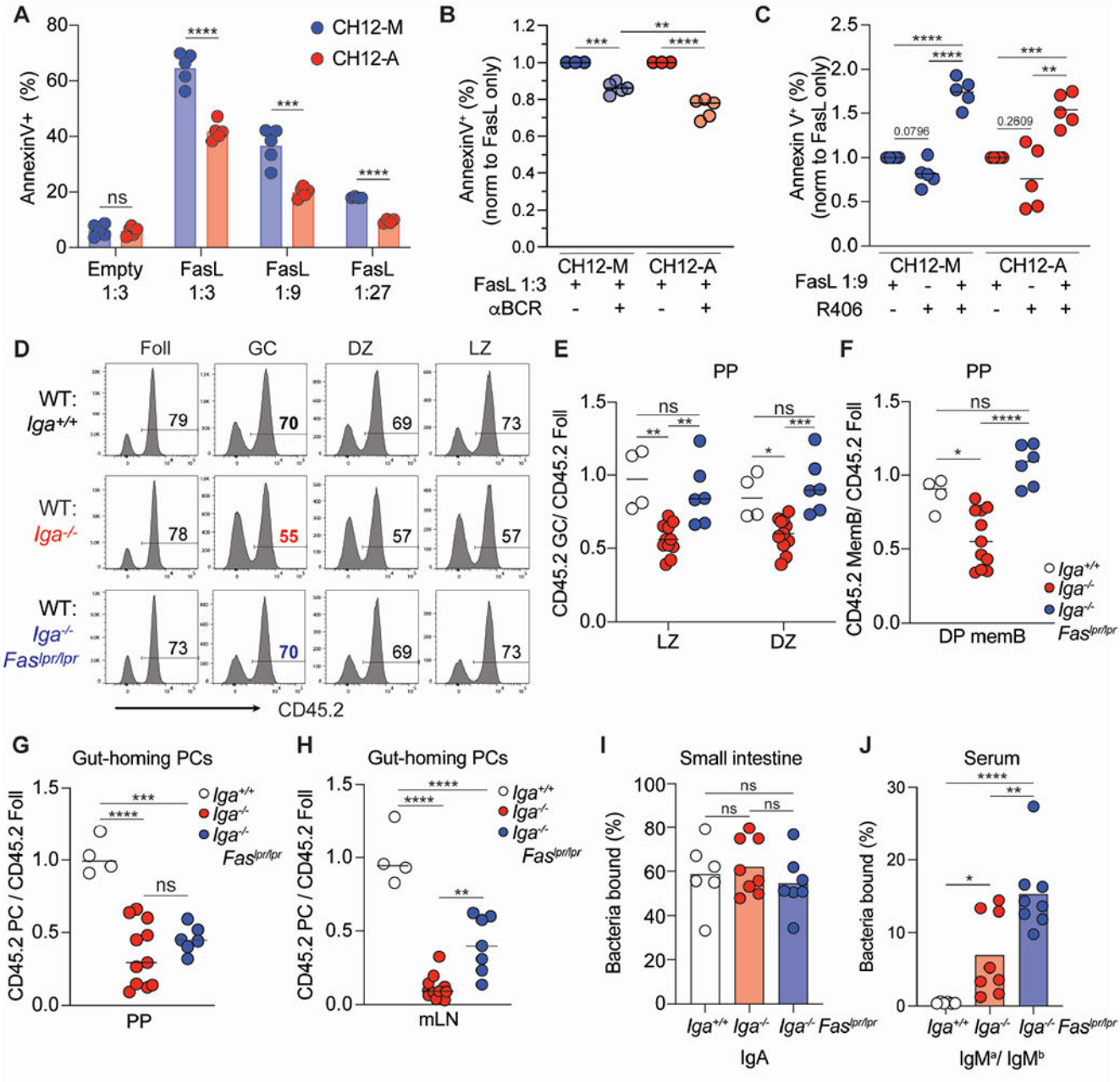

Figure 6. IgA$^+$ GC B cells are more resistant to Fas-dependent counter selection.

(A) Percentage of dead (defined as annexinV$^+$) CH12 cells 5 hours after incubation with FasL vesicles at indicated dilutions.

(B) Percentage of dead CH12 cells after BCR stimulation and incubation with FasL vesicles. Data is normalized to FasL vesicles alone.

(C) Percentage of dead CH12 cells after incubation with R409 and FasL vesicles. Data is normalized to FasL vesicles alone.

(D) Representative histograms of CD45 staining on mixed BM chimeras for indicated B cell populations.

(E) Ratio of frequency of CD45.2 LZ or DZ B cells to CD45.2 Foll B cells in PPs of mixed BM chimeras.
(F) Ratio of frequency of CD45.2 DP memory B cells to CD45.2 Foll B cells from PPs of mixed BM chimeras.
(G, H) Ratio of frequency of CD45.2 gut-homing PCs to CD45.2 Foll B cells from PPs(G) and mLN(H) of mixed BM chimeras.
(I, J) Mixed BM chimeras using μMT hosts to track antibodies using allotypic isotypes. (I) Percentage of endogenously coated small intestinal bacteria with IgA. (J) Percentage of intestinal commensal from μMT mice stained by IgM^a or IgM^b antibodies from mixed BM serum. Percentage shown as IgM^a/IgM^b ratio.
A-C are compiled data from at least 3 independent experiments. E-J are compiled data from 3 independent experiments with 1-3 mice per group (E-H) or 2-3 mice per group (I,J). ns=not significant, *$p < 0.005$; **$p < 0.001$; ***$p < 0.0005$; ****$p < 0.0001$. Unpaired two-tailed Student's t-test in A. One-way ANOVA in B, C, E-J.
See also Figure S6.

Key resources table

REAGENT or RESOURCE	SOURCE	IDENTIFIER
Antibodies		
Purified anti-mouse CD16/32, Clone 93	Biolegend	CAT# 101330; RRID:AB_2561482
BV711 anti-mouse B220, Clone RA3-6B2	Biolegend	CAT# 103255; RRID:AB_2563491
AF700 anti-mouse CD19, Clone 6D5	Biolegend	CAT# 115528; RRID:AB_493735
AF700 anti-mouse CD45.1, Clone A20	Biolegend	CAT# 110724; RRID:AB_493733
Pacific Blue anti-mouse CD45.1, Clone A20	Biolegend	CAT# 110722; RRID:AB_492866
BV650 anti-mouse CD45.1, Clone A20	Biolegend	CAT# 110736; RRID:AB_2562564
AF700 anti-mouse CD45.2, Clone 104	Biolegend	CAT# 109822; RRID:AB_493731
Pacific Blue anti-mouse CD45.2, Clone 104	Biolegend	CAT# 109819; RRID:AB_492873
BV650 anti-mouse CD45.2, Clone 104	Biolegend	CAT# 109836; RRID:AB_2563065
BV510 anti-mouse IgD, Clone 11-26c.2a	Biolegend	CAT# 405723; RRID:AB_2562742
PerCP/Cy5.5 anti-mouse IgD, Clone 11-26c.2a	Biolegend	CAT# 405710; RRID:AB_1575113
Pacific Blue anti-mouse IgD, Clone 11-26c.2a	Biolegend	CAT# 405712; RRID:AB_1937244
Alexa Fluor 647 anti-mouse IgD, Clone 11-26c.2a	Biolegend	CAT# 405708; RRID:AB_893528
BV421 anti-mouse CD138, Clone 281-2	Biolegend	CAT#142508;RRID:AB_11203544
AF647 anti-mouse GL7, Clone GL7	Biolegend	CAT# 144606; RRID:AB_2562185
PerCP/Cy5.5 anti-mouse GL7, Clone GL7	Biolegend	CAT# 144610; RRID:AB_2562979
PE/Cy7anti-mouse CD38, Clone 90	Biolegend	CAT# 102718; RRID:AB_2275531
PerCP/Cy5.5 anti-mouse CD73, Clone TY/11.8	Biolegend	CAT#127214;RRID:AB_11219403
BV605 anti-mouse CD80, Clone 16-10A1	Biolegend	CAT#104729;RRID:AB_11126141
BV605 anti-mouse CD86, Clone GL-1	Biolegend	CAT#105037;RRID:AB_11204429
FITC anti-mouse CD86, Clone GL-1	Biolegend	CAT# 105005; RRID:AB_313148
Biotin anti-mouse CXCR4, Clone 2B11/CXCR4	BD Biosciences	CAT# 551968; RRID:AB_394307
PE anti-mouse CXCR4, Clone 2B11/CXCR4	BD Biosciences	CAT# 551966; RRID:AB_394305
PE anti-mouse CCR9, Clone 9B1	Biolegend	CAT# 129708; RRID:AB_2073249
Biotin anti-mouse LPAM-1, Clone DATK32	Biolegend	CAT#120612;RRID:AB_11203892
APC anti-mouse IgM, Clone II/41	BD Biosciences	CAT# 550676; RRID:AB_398464
FITC anti-mouse IgM, Clone II/41	BD Biosciences	CAT# 553437; RRID:AB_394857
Biotin anti-mouse IgM, Clone II/41	BD Biosciences	CAT# 553436;RRID:AB_394856
FITC anti-mouse IgM^{a}, Clone MA-69	Biolegend	CAT# 408606; RRID:AB_940541
PE anti-mouse IgM^{a}, Clone MA-69	Biolegend	CAT# 408608; RRID: AB_940545
FITC anti-mouse IgM^{b}, Clone AF6-78	Biolegend	CAT# 406206; RRID: AB_315039
PE anti-mouse IgM^{b}, Clone AF6-78	Biolegend	CAT# 406208; RRID: AB_315041
FITC anti-mouse IgG1, Clone RMG1-1	Biolegend	CAT# 406605; RRID: AB_493292
PE ant-mouse IgG1, Clone RMG1-1	Biolegend	CAT# 406607; RRID:AB_10551439
FITC anti-mouse IgG2b, Clone RMG2b-1	Biolegend	CAT# 406705; RRID: AB_493296
PE anti-mouse IgG2b, Clone RMG2b-1	Biolegend	CAT# 406708; RRID:AB_2563381

REAGENT or RESOURCE	SOURCE	IDENTIFIER
Biotin anti-mouse IgG3, Clone RMG3-1	Biolegend	CAT# 406803; RRID: AB_315070
FITC anti-mouse IgA	Southern Biotech	CAT# 1040-02; RRID: AB_2794370
PE anti-mouse IgA	Southern Biotech	CAT# 1040-09; RRID: AB_2794375
Biotin anti-mouse IgA	Southern Biotech	CAT# 1040-08; RRID: AB_2794374
Biotin anti-active Caspase 3	BD Biosciences	CAT# 550557; RRID: AB_393750
AF700 anti-mouse Kappa	Biolegend	CAT# 409508; RRID:AB_2563583
APC anti-mouse CD22, Clone OX-97	Biolegend	CAT# 126110; RRID:AB_2561630
PerCP/Cy5.5 anti-mouse I-A/I-E, Clone M5/114.15.2	Biolegend	CAT# 107626; RRID:AB_2191071
PerCP/CY5.5 anti-mouse CD79b, Clone HM79-12	Biolegend	CAT# 132810; RRID:AB_2632918
PE/Cy7 anti-mouse CD69, Clone H1.2F3	Biolegend	CAT# 104512; RRID: AB_493564
AF700 anti-mouse CD4, Clone RM4-4	Biolegend	CAT# 116022; RRID:AB_2715958
PE anti-mouse Valpha2 TCR, Clone B20.1	BD Biosciences	CAT# 553289; RRID: AB_394760
Pacific Blue anti-mouse TCRbeta, Clone H57-597	Biolegend	CAT# 109226; RRID:AB_1027649
PE/Cy7anti-mouse Fas, Clone Jo2	BD Biosciences	CAT# 557653; RRID: AB_396768
FITC Annexin V	BD Biosciences	CAT# 556419; RRID: AB_2665412
PE anti-BTK (pY223), Clone N35-86	BD Biosciences	CAT# 562753; RRID:AB_2737769
AF647 anti-Syk (pY352), Clone 17A/P-ZAP70	BD Biosciences	CAT# 557817; RRID: AB_396884
PE anti-phosphotyrosine, Clone PY20	Biolegend	CAT# 309310; RRID:AB_2572196
AF647 anti-mouse CD98, Clone RL388	Biolegend	CAT#128210; RRID:AB_2254922
Biotin anti-mouse IgD , Clone 11-26c.2a	Biolegend	CAT# 405734; RRID: AB_2563344
Biotin anti-mouse CD138, Clone 281-2	Biolegend	CAT# 142512; RRID: AB_2561981
Biotin anti-mouse IgG2b, Clone RMG2b-1	Biolegend	CAT# 406704; RRID: AB_315067
Biotin anti-mouse CD8a, Clone 53-6.7	Biolegend	CAT# 100704; RRID: AB_312743
Biotin anti-mouse CD4, Clone GK1.5	Biolegend	CAT# 100404; RRID: AB_312689
Biotin anti-mouse IgG1, Clone RMG1-1	Biolegend	CAT# 406604; RRID: AB_315063
Biotin anti-mouse IgM^{a}, Clone MA-69	Biolegend	CAT# 408603; RRID: AB_940535
Purified anti-mouse IgM^{a}, Clone MA-69	Biolegend	CAT# 408602; RRID: AB_940549
Biotin anti-mouse IgM^{b}, Clone AF6-78	Biolegend	CAT# 406204; RRID: AB_315037
Purified anti-mouse IgM^{b}, Clone AF6-78	Biolegend	CAT# 406202; RRID: AB_315035
Unlabeled Goat anti-mouse IgA	Southern Biotech	CAT# 1040-01; RRID: AB_2314669
Unlabeled Goat anti-mouse IgG2b	Southern Biotech	CAT# 1090-01; RRID: AB_2794517
Unlabeled Goat anti-mouse IgM	Southern Biotech	CAT# 1020-01; RRID: AB_2794197
Biotin anti-mouse GL7, Clone GL7	Biolegend	CAT# 144616; RRID: AB_2721505
Rabbit Anti-RFP	Rockland	CAT# 600401379; RRID: AB_11182807
AF647 anti-mouse CD21/35, Clone 7E9	Biolegend	CAT#123424; RRID: AB_2629577
Mouse Anti-Phosphotyrosine, Clone 4g10	Millipore Sigma	CAT# 05-321; RRID: AB_309678
Mouse Anti beta-Actin, Clone AC-74	Millipore Sigma	CAT# A5316; RRID: AB_476743
HRP linked anti-mouse IgG	Cell Signaling	CAT# 7076; RRID: AB_330924
HRP conjugated anti-mouse Phospho-Tyrosine (p-Tyr-100)	Cell Signaling	CAT# 5465; RRID: AB_10694719

REAGENT or RESOURCE	SOURCE	IDENTIFIER
Purified mouse anti-actin, Clone C4/actin	BD Biosciences	CAT# 612657; RRID: AB_399901
Goat polyclonal anti-mouse IgD	Nordic Immunology	CAT# GAM/IgD(Fc)/7S
Rabbit polyclonal anti-RFP	Rockland	CAT# 601-401-379
Donkey anti-rabbit Cy3	Jackson Immunoresearch	CAT# 711-165-152; RRID: AB 2307443
Donkey anti-goat AF488	Jackson Immunoresearch	CAT# 705-545-003; RRID: AB_2340428
Human TruStain FcX	Biolegend	CAT# 422302; RRID:AB_2818986
PE/Cy7 anti-human CD19, Clone HIB19	Biolegend	CAT# 560728; RRID:AB_1727438
BV605 anti-human CD27, Clone O323	Biolegend	CAT# 302830; RRID:AB_2561450
APC anti-human CD10, Clone HI10a	Biolegend	CAT# 312210; RRID:AB_314921
APC/Cy7 anti-human CD10, Clone HI10a	Biolegend	CAT# 312212; RRID:AB_2146550
PerCP/Cy5.5 anti-human CD138, Clone MI15	Biolegend	CAT#356509; RRID:AB_2561898
PE Goat F(ab')2 Anti-human IgM	Southern Biotech	CAT# 2022-09; RRID: AB_2795614
PE Goat F(ab')2 Anti-human IgA	Southern Biotech	CAT# 2052-09; RRID: AB_2687523
Unlabeled Goat F(ab')2 Anti-human IgM	Southern Biotech	CAT# 2022-01; RRID: AB_2795610
Unlabeled Goat F(ab')2 Anti-human IgA	Southern Biotech	CAT# 2052-01; RRID: AB_2795709
FITC Goat F(ab')2 Anti-human IgG	Thermo Fisher	CAT#AHI1308;RRID:AB_1500723
Bacterial strains		
S. enterica strain SL1344 Δ*aroA* OVA	Gift from M. Bogunovic	N/A
Biological samples		
Frozen human tonsils	Gift from E. Clark	N/A
Chemicals, peptides, and recombinant proteins		
AF488 Streptavidin	Biolegend	CAT# 405235
PerCP/Cy5.5 Streptavidin	Biolegend	CAT# 405214
BV605 Streptavidin	Biolegend	CAT# 405229
BV650 Streptavidin	Biolegend	CAT# 405231
PE/Cy7Streptavidin	eBioscience	CAT# 25-4317-82
eFluor780 Live/Dead	BD Biosciences	CAT# 4302687
EF450 Live/Dead	eBioscience	CAT# 65-0863-18
DAPI	Thermo Fisher	CAT# 1306
Cholera Toxin	Sigma	CAT# C8052-2MG
16% PFA	Electrom microscopy sciences	CAT# 15710
DNase I	Sigma	CAT# DN25
Collagenase IV	Worthington	CAT# LS004189
Percoll	GE Healthcare	CAT# 17089101
FTY-720	Selleck Chemicals	CAT# S5002
Isotonic saline	Ricca Chemical	CAT# 7210-16
Ibrutinib	Selleckchem	CAT# S2680
R406	Invivogen	CAT# inhr406

REAGENT or RESOURCE	SOURCE	IDENTIFIER
Fluo 3 AM	Invitrogen	CAT# F23915
Fura Red	Invitrogen	CAT# F3021
5-Fluorouracil	Sigma	CAT# F6627
Recombinant Murine IL-3	Peprotech	CAT# 213-13
Recombinant Murine IL-6	Peprotech	CAT# 216-16
Recombinant Murine stem cell factor	Peprotech	CAT# 250-03
Lipofectamine 2000	Invitrogen	CAT# 11668-019
RIPA buffer	Thermo Fisher	CAT# 89900
4x Laemmli sample buffer	Bio-Rad	CAT# 1610747
Phosphatase inhibitor	Thermo Fisher	CAT# 1861281
BSA	Sigma	CAT# A2153
10% Mini-PROTEAN® TGX™ Precast Protein Gels	Biorad	CAT# 4561033
Protein Standard	BioRad	CAT# 161-0374
Trans-Blot Turbo Mini 0.2 μm PVDF Transfer Packs	BioRad	CAT# 1704156
ECL prime western blotting detection	GE Healthcare	CAT# RPN2232
SuperSignal West Pico Plus substrate	Thermo Fisher	CAT# 34577
4 to 12% NuPAGE Bis-Tris gels	Invitrogen	CAT# NP0322BOX
Restore PLUS Western blot stripping buffer	Thermo Fisher	CAT# 46430
Napthol AS-MX Phosphate	Sigma	CAT# N4875
N-N-Dimethylformamide	Fisher	CAT# D119-500
Levamisole	Sigma	CAT# L9756
Fast Blue B salt	Sigma	CAT# D9805
SIGMAFAST 3,3’-Diaminobenzidine tablets	Sigma	CAT# D4293
Critical commercial assays		
BRDU FITC kit	BD Biosciences	CAT# 559619
BD Cytofix/Cytoperm	BD Biosciences	CAT# 554714
EasySep Streptavidin RapidSpheres Kit	Stemcell Technologies	CAT# 19860A
SYBR green master mix	Biorad	CAT# 1725270
Fluoromount-G	Southern Biotech	CAT# 0100-01
Elisa/Elispot diluent solution	Invitrogen	CAT# 004202
Stop Solution for TMB Substrate	Biolegend	CAT# 423001
Deposited data		
N/A		
Experimental models: Cell lines		
NB-21	Gift from G. Kelsoe	Kuraoka et al., 2016
I29μ	Gift from C. Schrader	N/A
CH12	Gift from J. Muppidi	N/A
Platinum-E (Plat-E) retroviral packaging cell line	Gift from S. Schwab	N/A
Experimental models: Organisms/strains		

REAGENT or RESOURCE	SOURCE	IDENTIFIER
C57BL/6J (CD45.2)	The Jackson Laboratory	Strain# 000664 ; RRID: IMSR_JAX:000664
Ly5.2 (CD45.1) congenic B6.SJL-Ptprca Pepcb/BoyJ	The Jackson Laboratory	Strain# 002014; RRID: IMSR_JAX:002014
Rosa26-flox-stop-flox-tdTomato	The Jackson Laboratory	Strain# 007914; RRID: IMSR_JAX:007914
Aicda-cre	The Jackson Laboratory	Strain# 007770; RRID: IMSR_JAX:007770
B6.MRL-Fas^{lpr}	The Jackson Laboratory	Strain# 000482; RRID: IMSR_JAX:000482
B6J.Cg-Gt(ROSA)26Sor$^{tm95.1(CAG-GCaMPgf)Hze}$/MwarJ (gCAMP)	The Jackson Laboratory	Strain# 028865; RRID: IMSR_JAX:028865
B6.Cg-Tg(TcraTcrb)425Cbn/J (OTII)	The Jackson Laboratory	Strain# 004194; RRID: IMSR_JAX:004194
B6.Cg-Rag2$^{tm1.1Cgn}$/J	The Jackson Laboratory	Strain# 008449; RRID: IMSR_JAX:008449
B6.129SC-*Ighm*^{tm1Cgn}/J	The Jackson Laboratory	Strain# 002288; RRID: IMSR_JAX:002288
Iga$^{-/-}$	Barton Lab	N/A
IgM^{a}	Reboldi Lab	N/A
Rosa26-INDIA	Mayer Lab	N/A
cMYC-GFP	Bannard Lab	N/A
Oligonucleotides		
N/A		
Recombinant DNA		
MSCV-IRES-blc2	Gift from J. Muppidi	
Software and algorithms		
FlowJo	Tree Star	https://www.flowjo.com
FACSDiva	BD	https://www.bdbiosciences.com/en-us/products/software/instrument-software/bd-facsdiva-software
Prism	GraphPad Software	https://www.graphpad.com
ZEN 3.1	Carl Zeiss Microscopy	https://www.zeiss.com/microscopy/en/products/software/zeiss-zen.html
ImageJ	NIH	https://imagej.net/ij/index.html
Adobe Illustrator	Adobe Systems	https://www.adobe.com
Biorender	Biorender	https://www.biorender.com
Other		